Supporting Information

Chen et al.

SI Experimental Procedures

Chemicals and reagents. BI-D1870, BI-2536, volasertib, palbociclib hydrochloride, GDC-0941, SAR405 were purchased from Cayman Chemical. Insulin was purchased from Sigma Aldrich. Rapamycin and metformin hydrochloride were purchased from Abcam. N-acetyl-L-cysteine (NAC) was purchased from MP Biomedical. 1,2-dipalmitoyl-sn-glycero-3-phosphoserine, or DPPS, and D-myo-phosphatidylinositol 5-phosphate diC16, or PI(5)P, were purchased from Echelon Biosciences.

Protein purification, crystallization and structure determination. A construct of PI5P4Kα containing residues 33-405 was subcloned (Nde1, Xho1) from MGC-26205 clone into pET28a, which installed an N-terminal His-tag. The protein was expressed in *E. coli* BL21(DE3) cells and purified by metal affinity chromatography. After removing the His-tag by thrombin, the protein was further purified by gel filtration (1). A 20mg/ml protein solution in 20mM Tris-HCl pH 7.4, 500mM NaCl and 5mM DTT was used for hanging drop crystallization. Screen of commonly used kits identified two conditions that yielded large single crystals at room temperature: index G4 (0.2M Li_2SO_4, 0.1M HEPES pH 7.5, 25% PEG 3,350) and index F8 (0.2M $(NH_4)_2SO_4$, 0.1M HEPES pH 7.5, 25% PEG 3,350). Crystals were cryoprotected in 20% glycerol before being flash frozen in liquid nitrogen. To generate the complex with nucleotide, the crystal was soaked overnight in a pseudo-mother liquor supplemented with 1mM AMP-PNP and 2mM $MnCl_2$ before the cryoprotection steps. To generate complex with various inhibitors, 1mM compound was

used in all soaking steps (crystals were from the G4 condition). Diffraction data were collected at synchrotrons (APS 24-ID-C/E, SSRL BL14-1, NSLS X29) and processed using HKL2000 (2) (Tables S1 and S2). Molecular replacement using PDB entry 2ybx and refinement were performed using CCP4i (3), and graphic modeling was carried out in Coot (4). Models of small-molecule inhibitors were initially generated using the PRODRG server (5). All figures illustrating the crystal structures were generated by PyMOL.

The construct of human PI5P4Kβ used for crystallization (residues 32-416) was inserted into pET28a using the In-Fusion Cloning Kits (Clontech) from a synthesized full-length gene codon-optimized for *E. coli*. The protein was preceded by an N-terminal His-tag and PreScission protease site. Expression and purification were similar to those described for PI5P4Kα (except PreScission protease was used to remove His-tag). Co-crystallization with CC260 was achieved at room temperature using a sitting drop format: the protein solution contains 16mg/ml PI5P4Kβ, 20mM Tris-HCl pH 7.4, 0.5M NaCl, 5mM DTT and 1mM CC260; the well solution contains 20mM $CaCl_2$, 0.2M NaBr and 20% PEG 3,350. The apo protein was crystallized similarly except the well solution contains 0.15M DL-malic acid pH 7.0 and 20% PEG 3,350. Crystals were cryoprotected in 20% glycerol, and diffraction data were collected at APS 24-ID-C. The structure was solved by molecular replacement using PDB entry 1bo1(6) (Table S3). The human PI5P4Kγ construct, similarly purified, contains residues 32-421.

Purified PI5P4Kα^{33-405}, PI5P4Kβ^{1-416} and PI5P4K$^{32-421}$ (all with His-tag) were used for *in vitro* activity and binding assays and for high-throughput screening. All the mutants

were generated by QuikChange site-directed mutagenesis (Agilent Technologies) and purified similarly.

Chemical synthesis and characterization. Unless otherwise noted, all reagents were obtained from commercial suppliers and used without further purification (Fig. S6A). Reaction progress was monitored by UV/MS on an Agilent 6120 Quadrupole HPLC/MSD and Agilent 1260 Infinity. Organic extracts were dried over $MgSO_4$ and then concentrated under reduced pressure. Flash-column chromatography was performed on a Teledyne ISCO automated chromatography system using either normal phase RediSep Rf silica gel cartridges or reverse phase RediSep Rf 50g C18 silica gel cartridges. Methanol-d_4 and Chloroform-d_3 were obtained from commercial sources and used as received. NMR chemical shifts are reported in ppm relative to CD_3OD (3.31, 4.78 ppm ^1H and 49.0 ppm ^{13}C) and $CDCl_3$ (1.56, 7.26 ppm ^1H and 77.16 ppm ^{13}C). HRMS were obtained on an Agilent 6550 iFunnel QTOF LCMS.

(R)-8-Cyclopentyl-7-(cyclopentylmethyl)-2-((3,5-dichloro-4-hydroxyphenyl)amino)-5-methyl-7,8-dihydropteridin-6(5H)-one **(CC260)**. To a round bottom flask equipped with a stir bar was added **1a** (3.00 g, 19.1 mmol) in methanol (19 mL). The solution was cooled to 0 °C, and $SOCl_2$ (2.90 mL, 40.1 mmol) was added dropwise. The reaction mixture was then refluxed for 2 h and then concentrated. The remaining oil was diluted with *tert*-butyl methyl ether (20 mL) and stirred for 30 min at rt. The precipitate was filtered and washed with diethyl ether and dried under vacuum to give **2a (**3.77 g, quant.). The product was used in the next step without further purification. ^1H NMR (400 MHz, CD_3OD) δ 3.99 (t, J = 6.7 Hz, 1H), 3.84 (s, 3H), 2.06 – 1.79 (m, 5H), 1.76 – 1.54 (m, 4H), 1.09-

1.25 (m, 2H). ^{13}C NMR (101 MHz, CD_3OD) δ 171.32, 53.60, 37.91, 37.13, 33.39, 33.35, 26.04, 25.82. HRMS-ESI (*m/z*): $[M+H]^+$ calcd. for $C_9H_{17}NO_2$, 172.1337; found 172.1325.

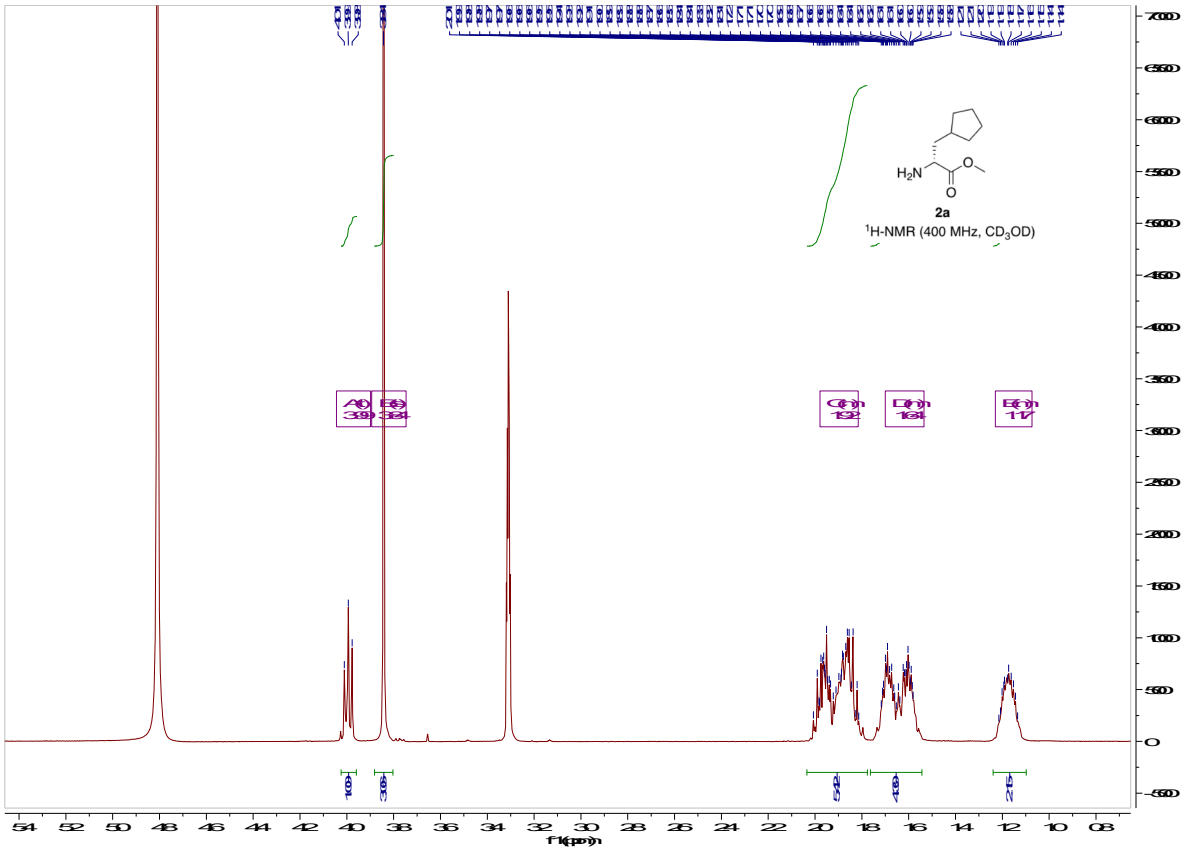

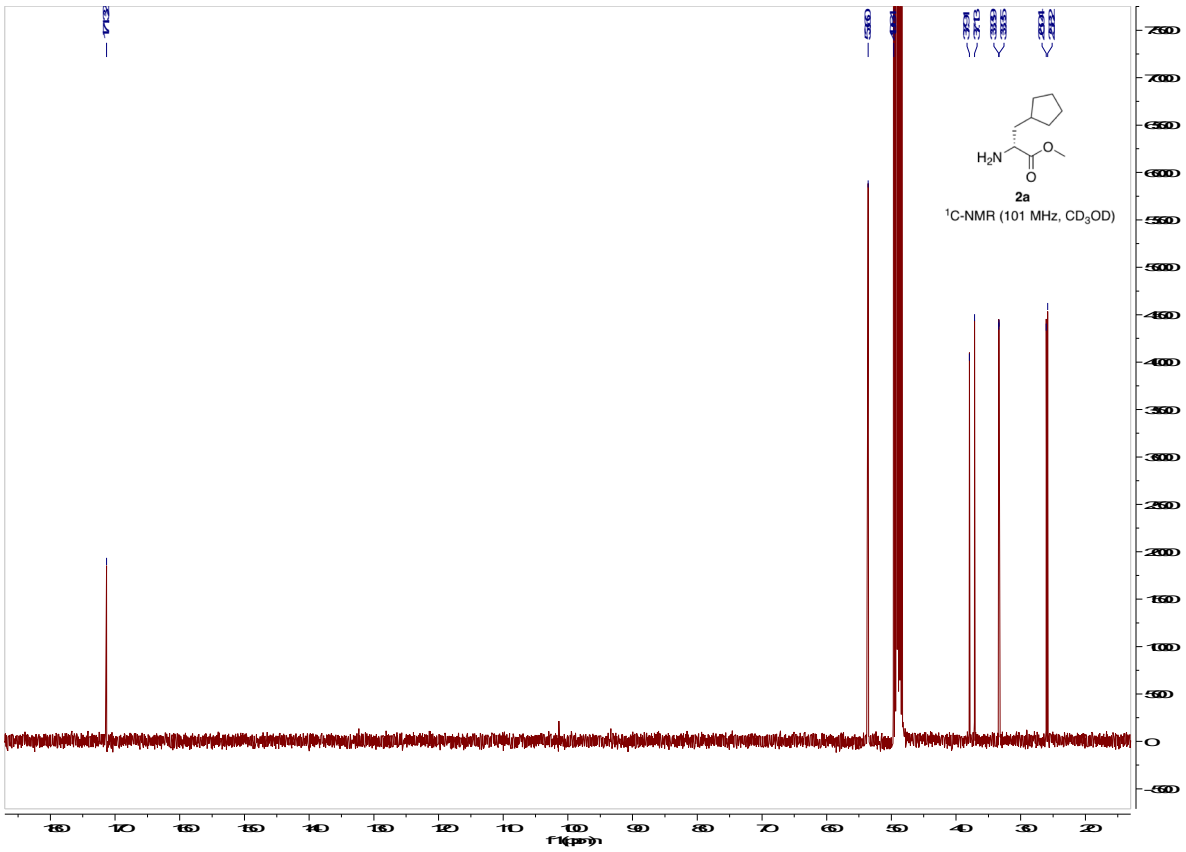

Methyl ester **2a** (3.77 g, 22 mmol) was dissolved in CH_2Cl_2 (37 mL) and cooled to 0 °C. Cyclopentanone (4.87 mL, 55 mmol), sodium acetate (1.86 g, 22.7 mmol), and sodium triacetoxyborohydride (6.90 g, 32.6 mmol) were subsequently added to the solution. The reaction mixture was stirred and allowed to warm to rt over 1 h. The reaction mixture was diluted with sat. $NaHCO_3$ and extracted with CH_2Cl_2. The organics were washed with water, dried, and concentrated to afford **3a** (4.95 g) which was used in the next step without further purification. ^{1}H NMR (400 MHz, CD_3OD) δ 3.76 (s, 3H), 3.34 (t, J = 7.9, 6.4 Hz, 1H), 3.01 (p, J = 6.9 Hz, 1H), 2.28 – 2.13 (m, 2H), 2.09 – 1.96 (m, 2H), 1.92 – 1.78 (m, 1H), 1.79 – 1.72 (m, 2H), 1.72 – 1.64 (m, 4H), 1.64 – 1.53 (m, 4H), 1.44 – 1.30

(m, 2H), 1.24 – 1.09 (m, 2H). HRMS-ESI (*m/z*): $[M+H]^+$ calcd. for $C_{14}H_{25}NO_2$, 240.1963; found 240.1954.

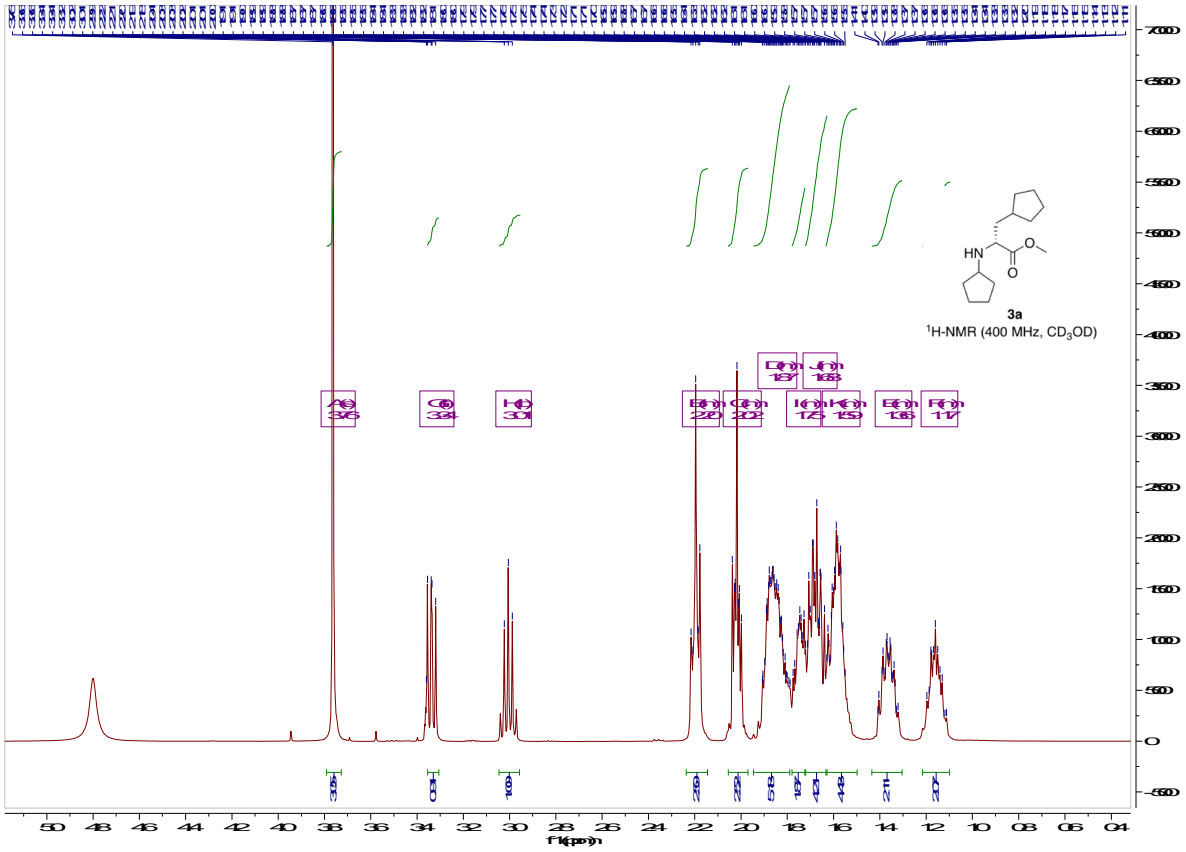

To a flame dried and N_2 flushed round bottom flask was added **3a** (4.81 g, 20.1 mmol) dissolved in dry acetone (50 mL). The solution was cooled to 0 °C, and then K_2CO_3 (3.06 g, 22.1 mmol) and 2,4-dichloro-5-nitropyrimidine (4.29 g, 22.1 mmol dissolved in acetone) were added. The reaction mixture was stirred overnight at rt. Solvent was removed under reduced pressure. The residue was diluted with water, extracted with ethyl acetate, dried and concentrated. The crude product was purified by silica gel column chromatography eluting with 0-30% ethyl acetate in hexane to give **4a** (2.01 g). The product was however still contaminated with some impurities that were removed during purification in the next step.

Next, **4a** (2.01 g, 5.08 mmol) was dissolved in glacial acetic acid (11.5 mL) and reacted with Fe powder (696 mg, 12.5 mmol). The reaction mixture was stirred for 4 h at 100 °C. The solution was filtered through Celite, and after concentration, the crude product was purified by silica gel column chromatography eluting with 0-60% ethyl acetate in hexane to give **5a** (1.40 g). ^{1}H NMR (400 MHz, CD_3OD) δ 7.58 (s, 1H), 4.32 – 4.14 (m, 2H), 2.12 – 1.39 (m, 17H), 1.31 – 0.93 (m, 2H). ^{13}C NMR (101 MHz, CD_3OD) δ 166.93, 154.35, 153.09, 139.00, 120.66, 61.71, 61.65, 40.54, 37.24, 34.53, 33.32, 30.39, 30.13, 26.16, 25.82, 25.25, 25.13. HRMS-ESI (*m/z*): $[M+H]^+$ calcd. for $C_{17}H_{23}ClN_4O$, 335.1638; found 335.1627.

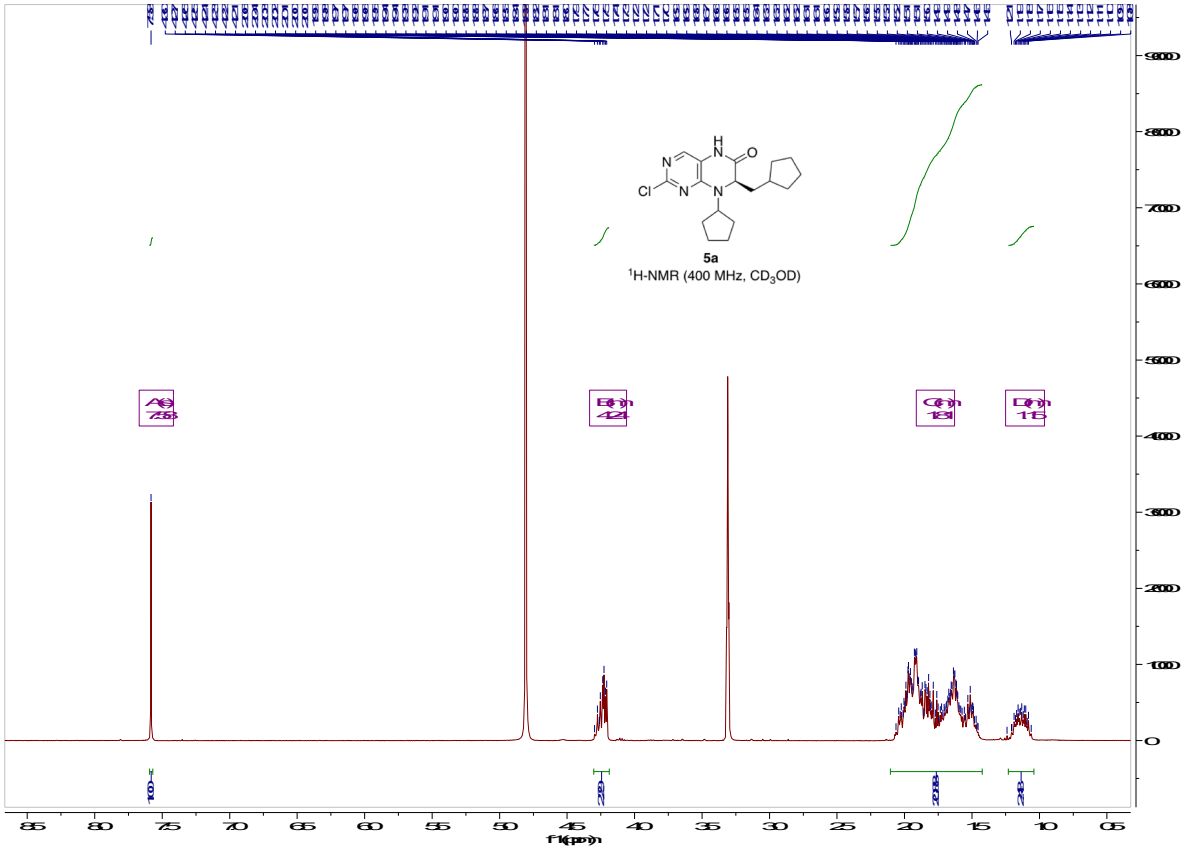

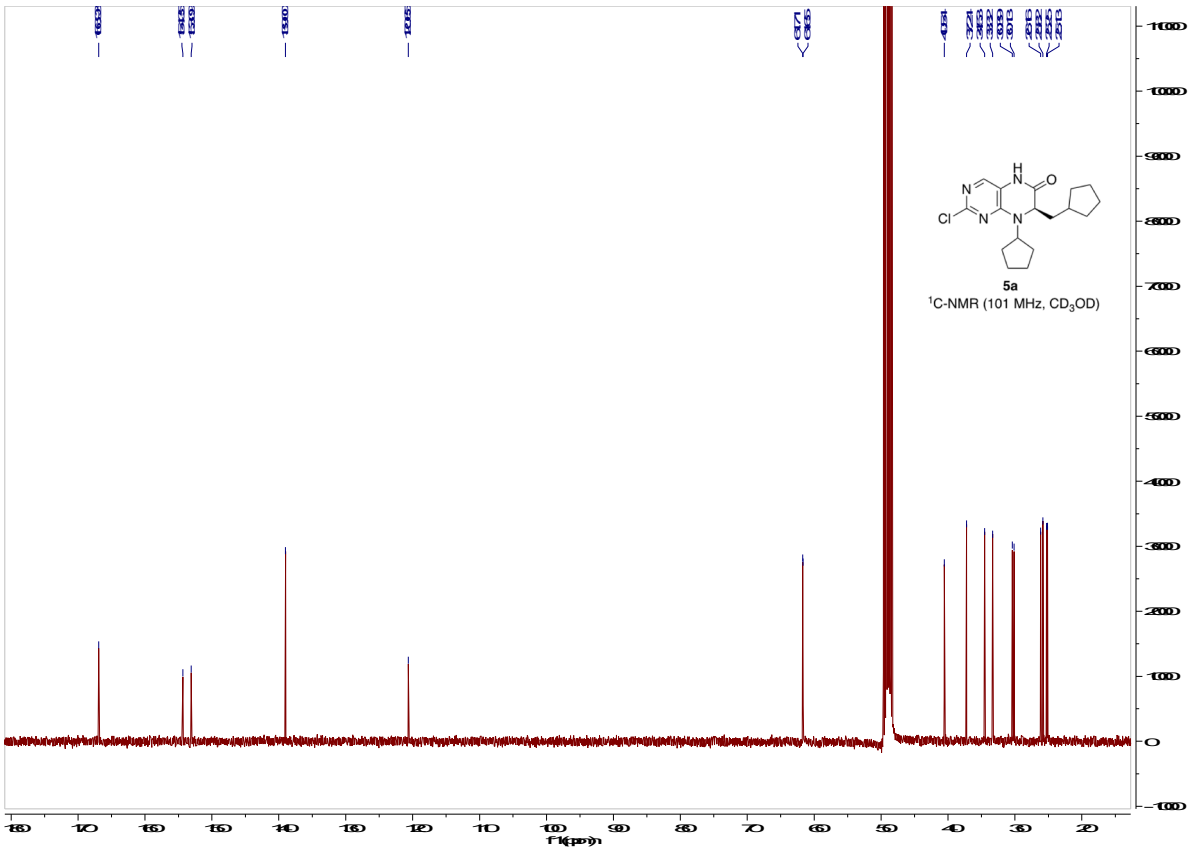

To a round bottom flask equipped with a stir bar and cooled to 0 °C was added **5a** (1.40 g, 4.18 mmol) in DMA (10 mL). NaH (125 mg, 5.43 mmol, 60% dispersion in mineral oil) and CH_3I (340 μL, 5.43 mmol) were subsequently added. The reaction mixture was stirred for 30 min at 0 ºC, and then for 2.5h at rt. The reaction was then quenched with cooled water, and the resulting mixture was extracted with ethyl acetate. The residue was washed with water three times. The organics was dried and concentrated. The crude product was purified by silica gel column chromatography eluting with 0-60% ethyl acetate in hexane to afford **6a** (1.00 g). ^{1}H NMR (400 MHz, $CDCl_3$) δ 7.68 (s, 1H), 4.38 (p, 1H), 4.21 (dd, J = 9.3, 4.0 Hz, 1H), 3.30 (s, 3H), 2.11 – 1.94 (m, 2H), 1.92 – 1.38 (m, 15H), 1.18 – 0.90 (m, 2H). ^{13}C NMR (101 MHz, $CDCl_3$) δ 163.87, 153.99, 152.51, 138.13,

121.61, 59.32, 59.25, 39.76, 36.02, 33.63, 32.23, 29.79, 29.64, 28.58, 25.37, 25.00, 24.10, 23.73. HRMS-ESI (*m/z*): $[M+H]^+$ calcd. for $C_{18}H_{25}ClN_4O$, 349.1795; found 349.1779.

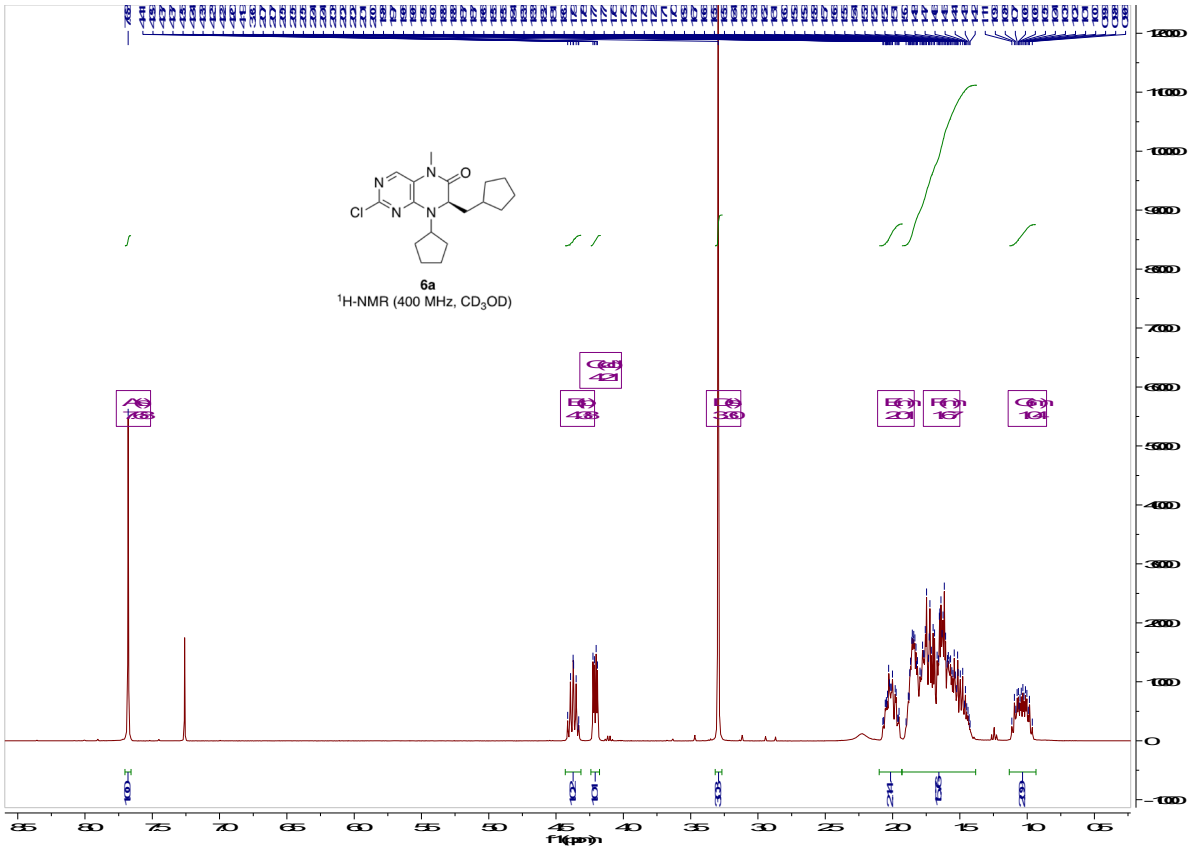

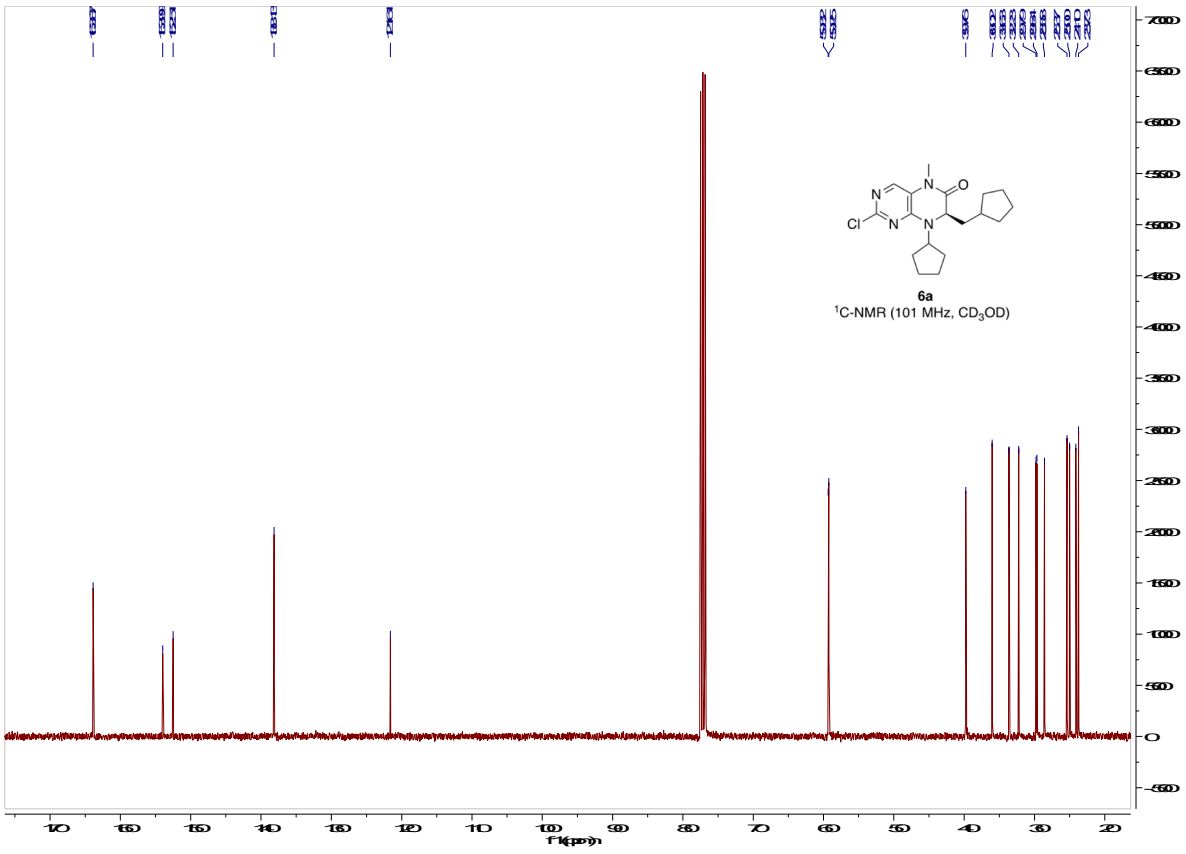

The enantiomeric purity of **6a** was determined using chiral HPLC analysis (Chiralpak IB, 90:10 hexanes:isopropanol, 1mL/min flow rate, detection at 250 nm) against its *(S)*-enantiomer. t_R of **6a** = 8.08 min; t_R of ***(S)*-6a** = 7.05 min. Chiral HPLC analysis showed that **6a** exists as a single enantiomer with >99:1 enantiomer ratio).

The methylated pteridine intermediate **6a** (330 mg, 1.0 mmol) and 4-amino-2,6-dichlorophenol (279 mg, 1.57 mmol) were suspended in a 1:4 mixture of ethanol and water. To this mixture was added conc. HCl (181 μL, 2.11 mmol), and the reaction mixture was refluxed overnight. The mixture was cooled down to rt, and the volatiles were evaporated. The crude product was then purified by reverse phase chromatography

(gradient elution: 10-100% MeCN in H_2O + 0.1% TFA) to yield **CC260** (380 mg) upon lyophilization.

Characterization of **CC260** (**for NMR spectra see, Fig. S6B, C**): ^{1}H NMR (500 MHz, CD_3OD) δ 7.54 (s, 1H), 7.44 (s, 2H), 4.43 (dd, J = 8.3, 3.6 Hz, 1H), 4.27 (m, 1H), 3.27 (s, 3H), 2.09 – 1.42 (m, 17H), 1.17 – 1.04 (m, 2H). ^{13}C NMR (151 MHz, CD_3OD) δ 164.60, 154.40, 150.97, 149.01, 130.50, 125.39, 124.24, 123.50, 117.73, 63.05, 61.80, 41.09, 36.85, 34.55, 33.02, 29.75, 29.72, 28.95, 26.28, 25.81, 24.36, 24.27. HRMS-ESI (*m/z*): $[M+H]^+$ calcd. for $C_{24}H_{29}Cl_2N_5O_2$, 490.1776, found 490.1776.

Preparation of *N,O*-dimethylated derivative of **CC260** and ***(S)*-CC260** for chiral HPLC analysis. To a 20 mL vial equipped with a stir bar and cooled to 0°C was added **CC260** (27 mg, 0.054 mmol) in DMF (1 mL). NaH (7 mg, 0.304 mmol, 60% dispersion in mineral oil) and CH_3I (19 mL, 0.304 mmol) were subsequently added. The reaction mixture was stirred for 10 min at 0ºC, and then for 30 min at rt. The reaction was then quenched with water, and the resulting mixture was extracted with ethyl acetate. The residue was washed with water three times. The combined organic layer was dried and concentrated. The crude product was purified by silica gel column chromatography eluting with 0-40% ethyl acetate in hexane to afford the ***N,O*-dimethylated derivative of CC260** (20 mg). A similar procedure was carried out to synthesize the ***N,O*-dimethylated derivative of *(S)*-CC260** (14 mg) using ***(S)*-CC260** (20 mg, 0.0408 mmol), NaH (5 mg, 0.217 mmol), and CH3I (13.5 µL, 0.217 mmol). The enantiomeric purity of the ***N,O*-dimethylated derivative of CC260** was determined using chiral HPLC analysis (Chiralpak AD-H, 90:10 hexanes:isopropanol, 1mL/min flow rate, detection at 254 nm) against its ***(S)*-enantiomer**. t_R of ***N,O*-dimethylated derivative of CC260** = 6.20 min; t_R

of **(S)-enantiomer** = 7.74 min. Chiral HPLC analysis of the dimethylated derivative established that **CC260** has high enantiomeric purity (>97/3 enantiomer ratio) (**see Fig. S7 for chiral HPLC traces**).

(R)-7-(Cyclohexylmethyl)-8-cyclopentyl-2-((3,5-dichloro-4-hydroxyphenyl)amino)-5-methyl-7,8-dihydropteridin-6(5H)-one **(CC314)**. **CC314** was prepared in a similar manner as described for **CC260** using **1b** (3.0 g, 17.5 mmol) to give **2b** (2.98 g). The entire amount of **2b** was converted to **3b** (4.18 g). The S_NAr reaction of **3b** yielded **4b** (2.49 g), which upon cyclization and methylation afforded **5b** (1.49 g) and **6b** (1.17 g), respectively. A portion of **6b** (200 mg, 0.551 mmol) was taken forward to give 254 mg of **CC314** after purification by reverse phase chromatography (gradient elution: 10-100% MeCN in H_2O + 0.1% TFA) and lyophilization.

Characterization of **CC314** by NMR and MS: ^{1}H NMR (500 MHz, CD_3OD) δ 7.55 (s, 1H), 7.44 (s, 2H), 4.44 (dd, J = 9.7, 4.0 Hz, 1H), 4.38 – 4.27 (m, 1H), 3.28 (s, 3H), 2.08 – 1.80 (m, 5H), 1.76 – 1.51 (m, 10H), 1.43 – 1.32 (m, 1H), 1.31 – 1.11 (m, 3H), 1.03 – 0.87 (m, 2H). ^{13}C NMR (151 MHz, CD_3OD) δ 164.55, 154.53, 151.37, 149.04, 130.56, 125.50, 125.16, 123.53, 117.90, 62.68, 59.95, 42.73, 35.23, 35.21, 33.35, 30.12, 29.91, 28.98, 27.35, 27.28, 27.05, 24.49, 24.24. HRMS-ESI (*m/z*): $[M+H]^+$ calcd. for $C_{25}H_{31}Cl_2N_5O_2$, 504.1933, found 504.1919.

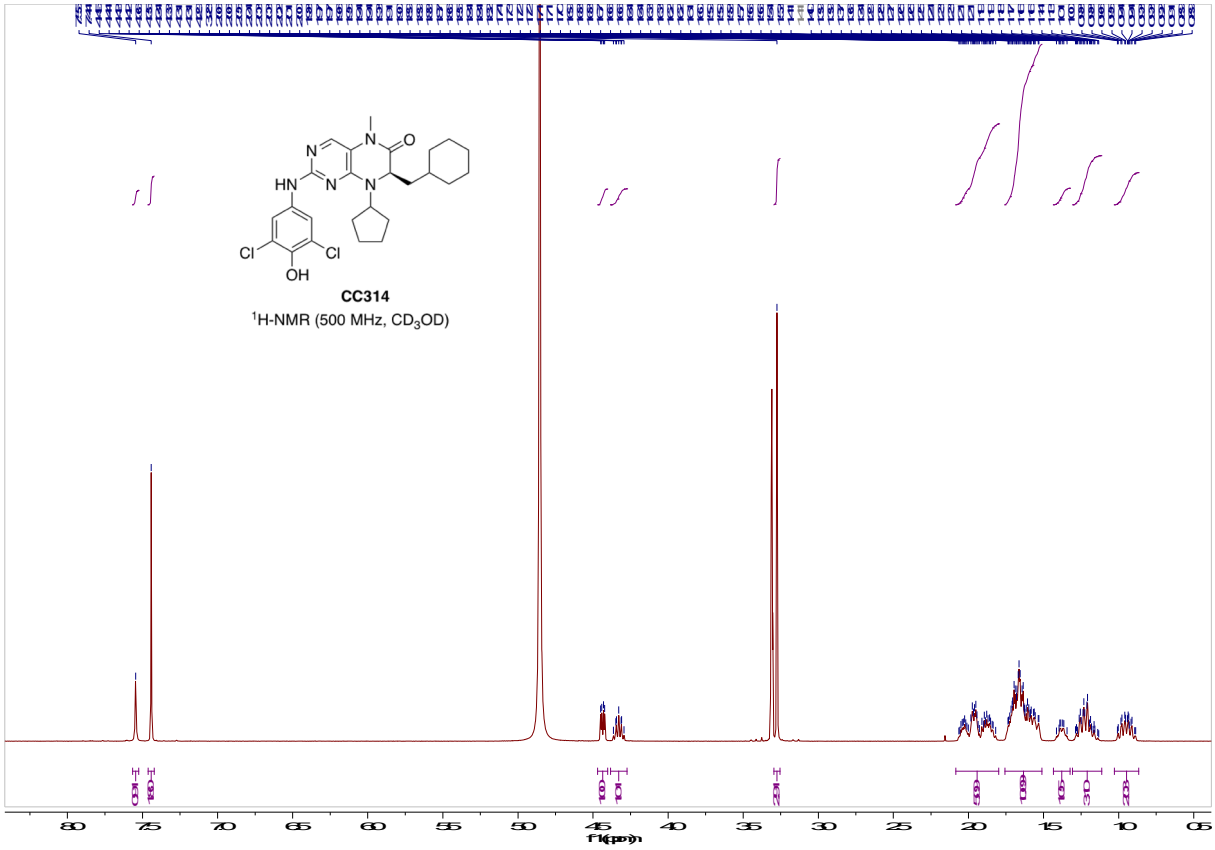
CC314
1H-NMR (500 MHz, CD3OD)
f1 (ppm)

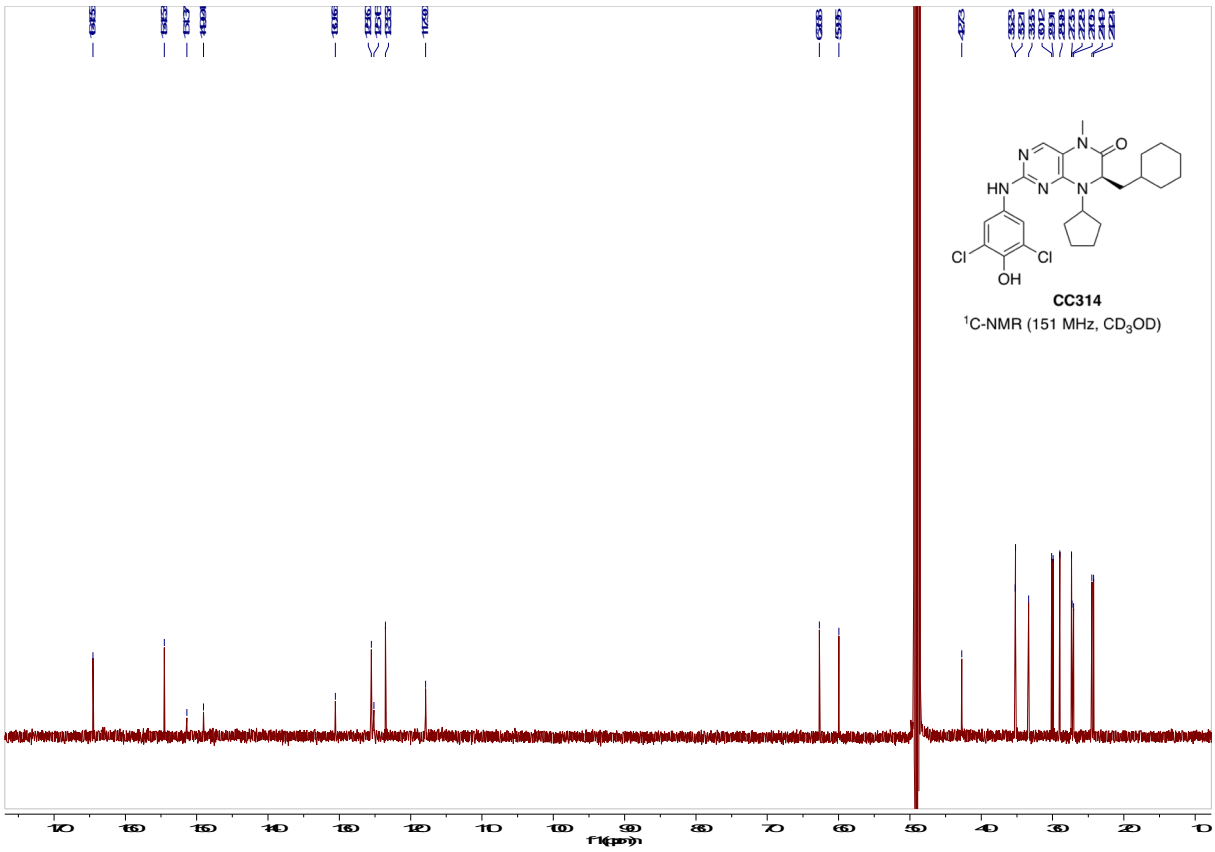

(R)-8-Cyclopentyl-2-((3,5-dichloro-4-hydroxyphenyl)amino)-7-isopropyl-5-methyl-7,8-dihydropteridin-6(5H)-one **(CC262)**. **CC262** was prepared in a similar manner as described for **CC260** using **1c** (1.0 g, 8.54 mmol) to give **2c** (1.01 g). The entire amount of **2c** was converted to **3c** (810 mg). The S_NAr reaction of **3c** yielded **4c** (220 mg), which upon cyclization and methylation afforded **5c** (110 mg) and **6c** (40 mg), respectively. **6c** (40 mg, 0.130 mmol) was reacted with 4-amino-2,6-difluorophenol (28.2 mg, 0.194 mmol) to give 11 mg of pure fractions of **CC262** after purification by reverse phase chromatography (gradient elution: 10-100% MeCN in H_2O + 0.1% TFA) and lyophilization.

Characterization of **CC262** by NMR and MS: ^{1}H NMR (600 MHz, CD_3OD) δ 7.47 (s, 1H), 7.13 – 7.05 (m, 2H), 4.29 (d, J = 3.5 Hz, 1H), 4.17 (m, 1H), 3.29 (s, 3H), 2.30 –

2.22 (m, 1H), 2.10 – 2.01 (m, 2H), 1.98 – 1.89 (m, 2H), 1.70 – 1.63 (m, 2H), 1.60-1.51 (m, 2H), 1.13 (d, J = 6.9Hz, 3H), 0.80 (d, J = 6.9, 3H). ^{19}F NMR (470 MHz, CD_3OD) δ -134.57. HRMS-ESI (m/z): $[M+H]^+$ calcd. for $C_{21}H_{25}F_2N_5O_2$, 418.2059; found 418.2056.

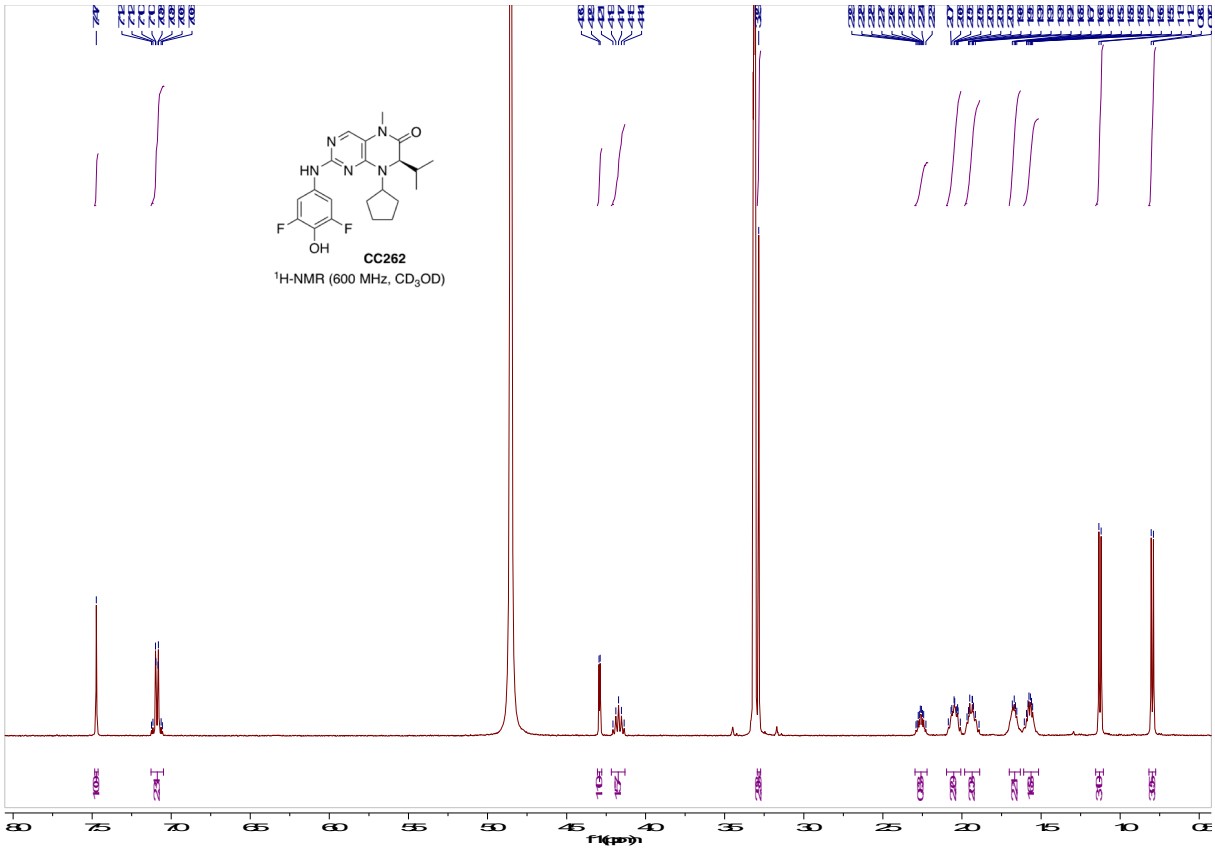

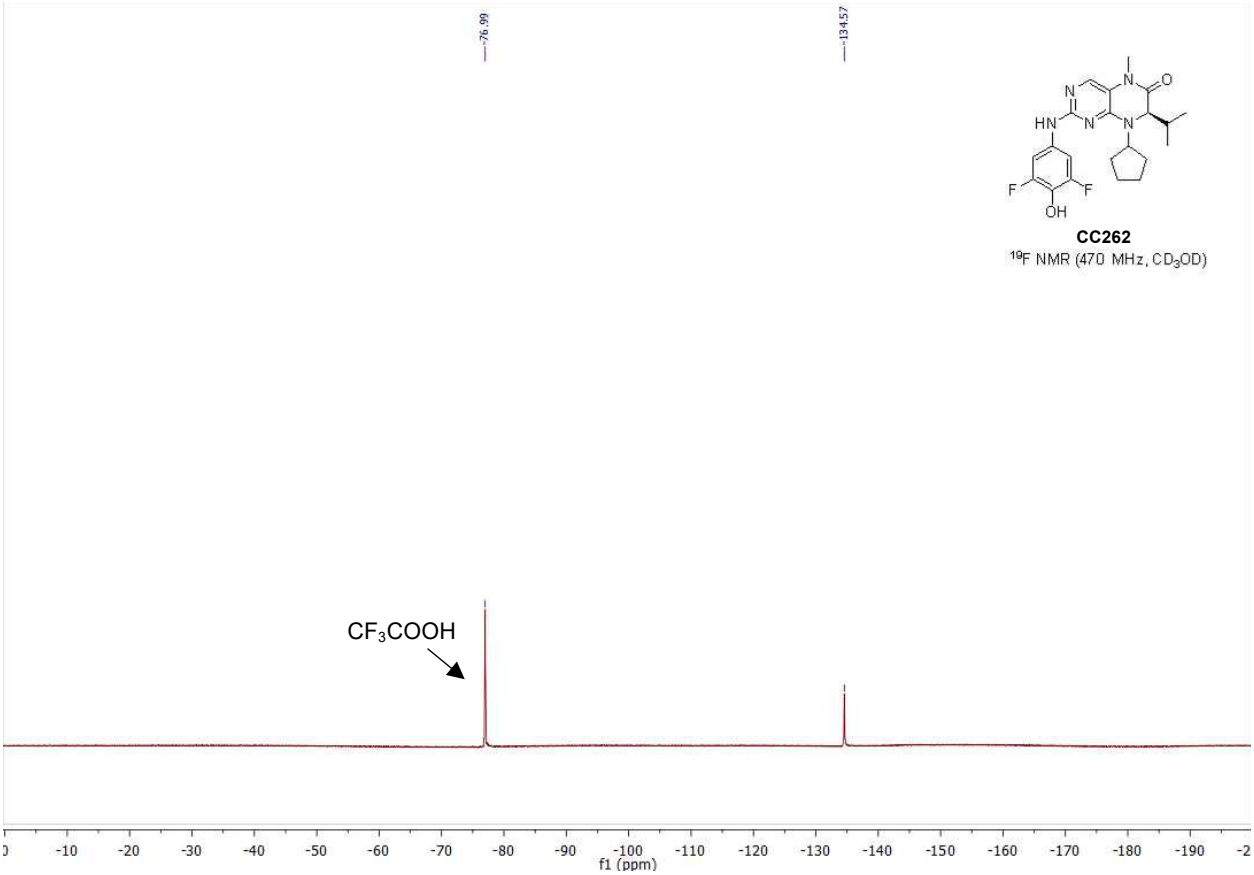

(R)-8-Cyclopentyl-2-((3,5-dichloro-4-hydroxyphenyl)amino)-7-isobutyl-5-methyl-7,8-dihydropteridin-6(5H)-one **(CC259)**. **CC259** was prepared in a similar manner as described for **CC260** using **1d** (12 g, 91.5 mmol) to give **2d** (15.9 g). The entire amount of **2d** was converted to **3d** (21.5 g). The S_NAr reaction of **3d** yielded **4d** (6.26 g), which upon cyclization and methylation afforded **5d** (2.16 g) and **6d** (1.17 g), respectively. A portion of **6d** (506 mg, 1.57 mmol) was taken forward to give 690 mg of **CC259** after purification by reverse phase chromatography (gradient elution: 10-100% MeCN in H_2O + 0.1% TFA) and lyophilization.

Characterization of **CC259** by NMR and MS: ^{1}H NMR (400 MHz, CD_3OD) δ 7.67 (s, 1H), 7.54 (s, 2H), 4.44 (p, J = 7.7 Hz, 1H), 4.32 (dd, J = 10.0, 3.9 Hz, 1H), 3.29 (s, 3H), 2.11 – 1.97 (m, 2H), 1.88 – 1.58 (m, 8H), 1.52 (m, 1H), 1.00 (d, J = 6.3 Hz, 3H), 0.88 (d,

J = 6.5 Hz, 3H). ^{13}C NMR (151 MHz, CD_3OD) *δ* 164.69, 154.31, 152.83, 147.92, 131.88, 129.17, 124.07, 123.41, 117.64, 61.88, 60.00, 43.60, 30.23, 30.10, 28.91, 25.85, 24.43, 24.13, 24.03, 21.81. HRMS-ESI (*m/z*): $[M+H]^+$ calcd. for $C_{22}H_{27}Cl_2N_5O_2$, 464.1620, found 464.1607.

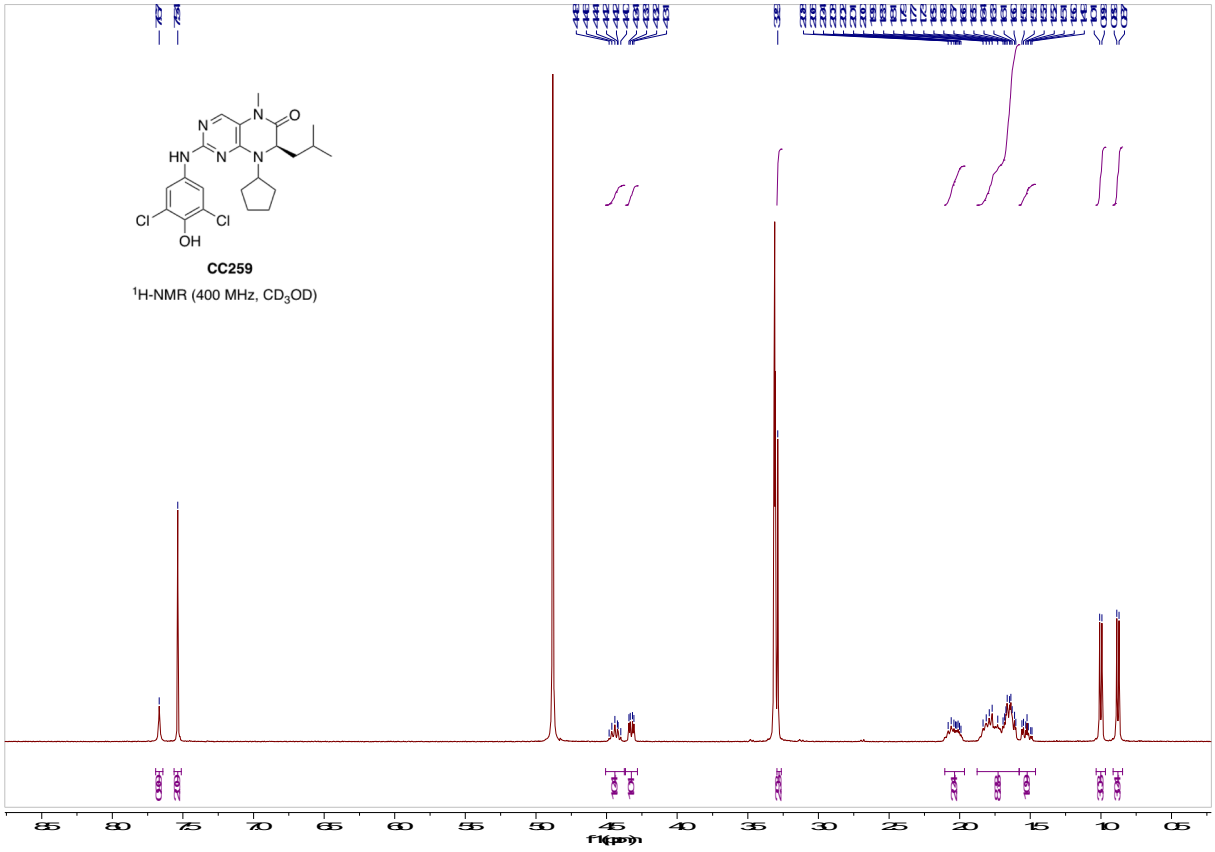

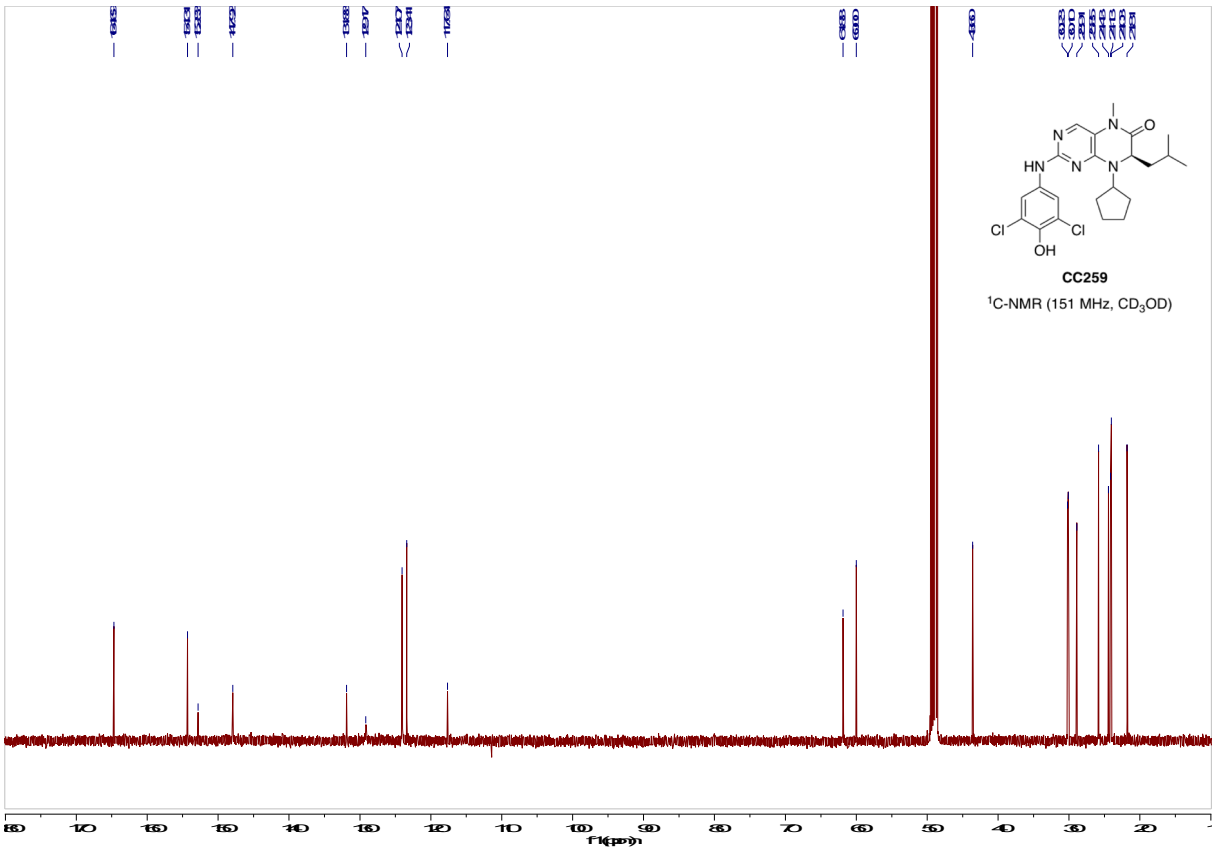

Cell culture, siRNA knockdown and mutant expression. BT474, MCF7, MDA-MB-157, MDA-MB-453, T47D breast cancer cells, C2C12 mouse myoblast cells, and HEK 293T cells were maintained in high-glucose DMEM medium containing 10% FBS. L6 rat myoblast cells were maintained in α-MEM medium containing 10% FBS. MCF-10A $p53^{+/+}$ and $p53^{-/-}$ cells were purchased from Horizon Discovery (HD 101-005) and cultured in DMEM/F12 medium supplemented with 5% horse serum, 20ng/ml EGF, 0.5μg/ml hydrocortisone, 100ng/ml cholera toxin and 10μg/ml insulin as recommended by the company. BT549 cells were maintained in RPMI-1640 medium containing 10% FBS. UACC-812 cells were cultured in RPMI-1640 medium with 20% FBS. MDA-MB-415 cells were culture in high-glucose DMEM medium containing 10% FBS and 10μg/ml insulin.

For differentiation into myotubes, C2C12 cells were kept in DMEM medium containing 2% horse serum for 5 days, and L6 cells were kept in α-MEM medium containing 2% FBS for 7 days. Amino-acid-free DMEM medium was prepared using powder from USBio, and MEM amino acids solution was from Gibco. Media were all supplemented with 100U/ml penicillin/streptomycin. Cell lines were purchased from ATCC.

BT474 cells were trypsinized and diluted to give 30%-50% confluence 24hrs after plating. Transfection of siRNA was achieved using Lipofectamine RNAiMAX reagent (Invitrogen) following manufacturer's protocol. A final siRNA concentration of 50nM was used in reverse transfection. The siRNAs used are summarized below:

Oligo name	Source	siRNA ID or sequence	Target
siPIP4K2A/B	Sigma Aldrich	UUGAUCAUCAAUUCCAAACCUC	NM_005028/NM_003559
siPIP4K2B	Sigma Aldrich	CCCUCGAUCUAUUUCCUUCUU	NM_003559
siPIP4K2A	Sigma Aldrich	CUGCCCGAUGGUCUUCCGUAA	NM_005028
siControl	Sigma Aldrich	SIC001	

Lentivirus was used to generate BT474 cell lines that stably express wildtype and mutant PI5P4Kβ. HEK 293T cells were used for lentiviral amplification. PI5P4Kβ wildtype and double mutant (V148F/T201M) were cloned into pLVX-IRES-Puro lentiviral vector (Clontech) along with a Kozak sequence and a 3x-Flag-tag at the N-terminus using the in-fusion cloning reagents (Clontech). The expression plasmid, along with pMLV-Gag-Pol and pVSV-G plasmids, were transfected into HEK 293T cells. Viruses were collected 48hrs after transfection and filtered. BT-474 cells were infected in the presence of 8μg/ml polybrene (EMD Millipore), and stable lines were selected in basal media supplemented with 1μg/ml puromycin (Gebico). Protein expression was confirmed by western blot with anti-Flag antibody (Cell Signaling Technology).

Immunoblot analysis. After wash with cold DPBS buffer, cells were lysed in RIPA buffer that contains 50mM Tris-HCl pH 8.0, 150mM NaCl, 1mM EDTA, 1mM EGTA, 1% NP-40, 0.5% sodium deoxycholate, 0.1% SDS, and protease and phosphatase inhibitor cocktails (Roche). Total protein concentrations were measured using the BCA assay (Thermo scientific). Cell lysate (about 80μg protein) was resolved by SDS-PAGE and blotted onto PVDF membranes. The membranes were probed overnight at 4°C with appropriate primary antibodies and incubated with secondary fluorescent antibodies (LI-COR Biosciences) for 1hr at room temperature before imaging by an Odyssey CLx system. Anti-p53 primary antibody was purchased from Sigma Aldrich. Anti-PI5P4Kγ antibody was purchased from Proteintech Group. All the others, including those targeting PI5P4Kα and PI5P4Kβ, were purchased from Cell Signaling Technology.

Adenine nucleotides measurement. BT474 cells were plated on white solid-bottom 96-well plates in sextuplicate (corning 3917; $2x10^4$ cells per well). C2C12 cells were plated and differentiated on the same type of plates. After treatment with compound overnight, total cellular ATP levels were measured by a luminescent ATP detection assay kit (Abcam) following manufacturer's protocol and normalized against the total protein concentration.

To measure nucleotide concentration using HPLC or LC-MS/MS, cells were rinsed three times with ice-cold DPBS buffer at room temperature and lysed in ice-cold 0.4M perchloric acid (500μl acid per 10^6 cells). The culture dishes were sealed and transferred to a -80°C freezer. Cell lysates were then thawed on ice, scraped off, and centrifuged at

14,000rpm at 4°C for 10min. The pellet was solubilized in 0.2M NaOH and set aside for measurement of protein concentration. The supernatant was transferred to clean tubes and neutralized with 3M $KHCO_3$. The neutralized sample was kept on ice for 10min and then transferred to a -80°C freezer. After 2hrs, thawed sample was centrifuged again to remove the precipitated perchlorate, filtered, adjusted according to protein concentration, aliquoted and stored at -80°C. The sample was thawed on ice just before the HPLC or LC-MS/MS experiment. For HPLC experiments, the sample was analyzed on an Agilent 1200 HPLC system equipped with Luna C_{18} (150mm x 4.6mm, 3μm, 100Å; Phenomenex). The flow rate was 0.7mL/min. Nucleotide separation was performed with two buffers (buffer A and B) following a literature procedure (7). The gradient was 0-5min, 100% A; 5-20min, 0-100% B; 20-25min, 100% B; 25-30min, 100% A for column re-equilibration. For LC-MS/MS experiment, sample (and AMP, ADP and ATP standards) was applied to an Agilent 1290 Infinity LC System equipped with a Hypercarb column (100mm x 4.6mm, 5μm; ThermoFisher Scientific) and coupled to an Agilent 6490 Triple Quad LC/MS. The nucleotides were separated using 20mM ammonium acetate in water (solvent A) and 5% acetonitrile in water buffered with 20mM ammonium acetate (solvent B), which were both adjusted with ammonium hydroxide to pH 9.0. The flow rate was 0.7mL/min, and the column temperature was maintained at 35ºC. The gradient elution program was: 0–2min, 0-5% B; 2–12min, 5–10% B; 12–22min, 10-20% B; 22–25min, 20-100% B; 25-30min, 100% B, and then back to 100% A for 1min, which was maintained for another 9min to recondition the column. Mass spectrometric ESI ionization was performed in the negative ion mode and the source parameters were set as follows: gas temperature, 200ºC; gas flow, 12L/min; nebulizer pressure, 35psi; sheath gas temperature, 200ºC; sheath gas

flow, 12L/min; capillary voltage, -4,000V; fragmentor voltage, 380V. Quantification and confirmation of each compound was performed in the multiple reaction monitoring (MRM) mode (Fig. S11D).

PI(5)P measurement. BT-474 cells were seeded onto 10cm dishes at ~60% confluency. After incubation with 10μM CC260 or DMSO overnight, cells were collected, and cellular phosphoinositides were purified using NeoBeads (Echelon Biosciences; 3mg beads for each plate of cells). After neomycin affinity chromatography (8), the lipid solution was dried under nitrogen using a SpeedVac. The dried lipids were resuspended and sonicated in 100μl buffer containing 50mM Tris (pH 7.4) and 1mM EGTA. PI(5)P was converted to ^{32}P-labeled PI(4,5)P_2 in a 50μl reaction mixture containing 20μl resuspended lipids, 20mM HEPES (pH 7.3), 10mM $MgCl_2$, 20μM ATP, 10μCi [γ-^{32}P]-ATP, and 4μg/ml PI5P4Kα (I143F/T196M double mutant) for 3 hours at room temperature (9). Radiolabeled PI(4,5)P_2 was quantified with a phosphoimager after TLC, and the amount of PI(5)P was normalized against total protein concentration.

ROS and cell growth rate. 2',7'–dichlorofluorescin diacetate (DCFDA) was used to assess intracellular ROS levels. DCFDA is deacetylated in the cell and oxidized by ROS to a fluorescent product 2',7'-dichlorofluorescein (DCF). BT-474 cells were plated on a black clear-bottom 96-well plate (Corning 3603; 2x10^4 cells per well). ROS was measured by a DCFDA cellular ROS detection assay kit (Abcam) following the manufacturer's protocol. The cells were treated with compound for 6hrs before fluorescence was measured using a SpectraMax M5 plate reader (excitation 485nm, emission 535nm).

To measure cell number using the CellTiter-Glo 2.0 assay kit (Promega), cultured cells were equilibrated to room temperature for 30min, and an equal volume of the CellTiter-Glo reagent was added and mixed for 2min on an orbital shaker. The plates were incubated for another 10min before luminescence was recorded using a SpectraMax M5 plate reader. To assess the effect of compound on growth, cells were plated onto white solid-bottom 96-well plates (corning 3917) in sextuplicate and treated with CC260 or DMSO for either 24hrs or 48hrs. The media were then replaced with fresh media without the compound. After 24hrs of washout, cell numbers were determined at 0, 24, 48, and 72 hrs.

Seahorse XF real-time ATP rate Assay. Assessment of mitochondrial and glycolytic functionality was performed by a Seahorse XF96 Analyzer (Agilent Technologies, Santa Clara, CA) using the XFp Real-Time ATP Rate Assay Kit. C2C12 myoblasts were seeded at 12,000 cells per well in the Seahorse XF microplate and differentiated for 5 days. BT-474 cells were seeded at 20,000 cells per well in complete culture medium. Cells were treated with either DMSO or 10μM CC260 overnight in high-glucose DMEM medium. One hour before measurement, the culture medium was replaced with the assay medium (Seahorse XF DMEM medium, pH 7.4, supplemented with 10mM glucose and 2 mM glutamine). After measuring basal respiration, 1.5 μM oligomycin (final concentration) and 0.5μM rotenone/antimycin A were sequentially injected. Data were normalized to protein content in each well determined by the BCA assay and analyzed by *Wave* software (Agilent Technologies).

SI Figure Legends

Figure S1. The hit molecules are competitive with ATP binding to PI5P4Kα. (**A**) The Lineweaver-Burk plot of the enzyme kinetic data shown in Fig. 1B. (**B**) The concentration-inhibition curves for the hit molecules based on ADP-Glo™ assay. Experiments were performed in triplicate at a constant ATP concentration of 10μM. For PI5P4Kα, $K_{m,\ ATP}$ was determined to be ~13μM based on data shown in Fig. 1B.

Figure S2. Crystallographic analysis reveals the structure of the specificity loop. PI5P4Kα crystals were obtained from two conditions. In both forms, extensive electron density in the shape of an α-helix was observed that corresponds to the N-terminal portion of the specificity loop. The helix has been predicted by sequence analysis (10), and by NMR study (11), but was not seen in a previously determined structure (pdb: 2YBX). (**A**) A ribbon diagram of PI5P4Kα dimer with the protomers colored green and blue. The specificity loops are highlighted in yellow. Four sulfate ions, shown as space filling models, are found near the 2-fold symmetry axis on a flat surface facing toward the membrane, which mark possible binding sites for the acidic head groups of phospholipids. (**B**) The Cα trace of one protomer. The difference map, contoured at 2.5σ and shown in green, indicates the position of the specificity loop. (**C**) Glu-150 and Glu-154 form multiple hydrogen bonds with the amino-terminal region of the specificity loop, stabilizing the sharp turn from the β-strand (β12) to the helix. This structural feature is likely unique to PI5P4Ks since Glu-150 and Glu-154 are highly conserved only in type 2 kinases. The turn may explain PI5P4Ks' substrate specificity because it is incompatible with the binding mode of PI(4)P (1), the substrate for type 1 kinases. Although PI(4)P is much more abundant

in a cell, type 2 kinases cannot phosphorylate them. (**D**) and (**E**) The orientation of the helix, likely influenced by crystal packing, is slightly different between the two apo structures (2FoFc maps contoured at 1σ). It is possible that the helix may adopt yet another orientation when the protein is laterally associated with the membrane (11).

Figure S3. The binding mode of ATP. (**A**) 2FoFc map around the bound ATP analog and Mn(II) ions (contoured at 1σ). (**B**) The details of the binding interactions between AMP-PNP/$Mn(II)_2$ and PI5P4Kα. Hydrogen bonds are shown as dashed lines. Red spheres represent water. Blue spheres represent Mn(II) ions. The structure of PI5P4Kα:AMP-PNP complex is similar to that of zebrafish PI4P5Kα (1), a type 1 kinase, but offers higher resolution. (**C**) and (**D**) The difference between the PI5P4Kα structure and a published PI5P4Kβ:AMP-PNP structure may be related to the fact that the latter does not contain any metal ions (pdb: 3X03) (12). Like protein kinases, divalent metal ions are required for lipid kinase activity. In PI5P4Kα, Asp-359 from the conserved “IID” motif serves a similar function of metal binding as the aspartate from the “DFG” motif of protein kinases (1). It becomes also clear from the high-resolution structure that there is no salt bridge, or water-mediated hydrogen bonds, between Lys-145 and Asp-151, a significant difference from protein kinase, which we explored in the synthesis of lipid-kinase-specific inhibitors. In one of the AMP-PNP structures, the Gly-rich loop is partially visible. However, the loop does not appear to make extensive contacts with β- and γ-phosphates of the bound ATP analog, which is again different from its counterpart in protein kinases.

Figure S4. Details of the binding interactions between the hit molecules and PI5P4Kα. Hydrogen bonds are shown as dashed lines with bond lengths indicated. Waters are shown as red spheres. In the apo structure, the backbone amide groups of Asp-359 and Ile-360 attract two water molecules, WAT1 and WAT2, which are hydrogen bonded to a chain of other well-ordered water molecules within the active site. WAT1 is displaced by a carbonyl oxygen of the bound compounds. In the complex with palbociclib, Asp-125 from the Gly-rich loop undergoes a conformational change to engage the piperazine side chain of the compound.

Figure S5. A PIPK-specific hydrophobic pocket. (**A**) The details of BI-2536 binding to protein kinase Plk1 (13) (pdb: 2RKU). The 6-carbonyl oxygen of the inhibitor engages in water-mediated hydrogen bonds with Lys-82, as well as backbone amide groups of Asp-194 and Phe-195. The salt bridge between Lys-82 and Glu-101 is present in all protein kinases. (**B**) Surface representation of the inhibitor binding pocket in Plk1. (**C**) Surface representation of the inhibitor binding pocket in PI5P4Kα. The red asterisk marks the entry point to the hydrophobic pocket that is present only in this family of lipid kinases.

Figure S6. Chemical synthesis and characterization. (**A**) Reagents and conditions: (i) $SOCl_2$, CH_3OH, 0 °C to reflux, 2 h; (ii) cyclopentanone, CH_3COONa, $Na(CH_3COO)_3BH$, CH_2Cl_2, 0 °C to rt; (iii) 2,4-dichloro-5-nitropyrimidine, K_2CO_3, acetone, 0 °C to rt, overnight; (iv) Fe powder, CH_3COOH, 80 °C; (v) 1. NaH, *N*,*N*-dimethylacetamide, 0 °C, 20 min, 2. CH_3I, 0 °C to rt; (vi) aminophenol derivatives, CH_3CH_2OH/H_2O, conc. HCl, reflux,

overnight. (**B**) ^{13}C NMR spectrum (151 MHz, CD_3OD) of CC260. (**C**) ^{1}H NMR spectrum (500 MHz, CD_3OD) of CC260.

Figure S7. HPLC chromatograms of CC259, CC260, CC314 and CC262 on a ZORBAX SB-C18 column (2.1x50mm, 1.8mm); flow rate: 0.2mL/min; 0% to 100% of 0.1% TFA in CH_3CN over 35min; detection was performed at two UV wavelengths. The asterisks indicate the solvent front.

Figure S8. Determination of enantiomeric purity of CC260. In order to determine the enantiomeric purity of CC260, the enantiomer of CC260 was prepared according to Fig. S6A starting from the *(S)* enantiomer of the starting amino acid **1a**. Chiral separation of CC260 and *(S)*-CC260 was not possible with chiral HPLC chiral columns and conditions. Therefore, a derivative of CC260 with both acidic *–NH* and *–OH* methylated was prepared [see Chemical synthesis and characterization in Materials and Methods section]. The *N,O*-dimethylated derivative was also prepared for the *(S)*-CC260. Chiral HPLC analysis of the *N,O*-dimethylated derivative of CC260 using the Chiralpak AD-H established high enantiomeric purity (95% ee). (**A**) A mixture of *N,O*-dimethylated derivatives of CC260 and *(S)*-CC260 (90:10 hexanes:isopropanol, 1mL/min, 254nm). (**B**) *N,O*-Dimethylated derivative of CC260. (**C**) *N,O*-Dimethylated derivative of *(S)*-CC260.

Figure S9. Determining the K_is for the newly synthesized inhibitors. (**A**) Autoradiographs of the TLC plates over a range of ATP concentrations (a duplicate is shown). Based on

the titration, the $K_{m,ATP}$ values for PI5P4Kα and PI5P4Kβ were determined to be 13μM and 17μM, respectively. Published $K_{m,ATP}$ values for PI5P4Kβ vary widely (6μM (14), 67μM (15), 236μM (12)), and the reason behind the discrepancy is not clear at this time. (**B**) Representative autoradiographs comparing concentration effect relationship of CC260 with that of parent compound BI-D1870. In this experiment, ATP concentration was fixed at 20μM. (**C**) and (**D**) Concentration effect curves obtained at 20μM ATP. The K_i values for CC259, CC260 and CC314 against PI5P4Kβ were obtained from titrations at a higher ATP concentration (60μM), which shifts IC_{50} to the right (insert): the concentration of PI5P4Kβ in the assay mixture was about 40nM, which was not negligible at low compound concentrations. All experiments were performed in triplicate.

Figure S10. CC260 does not potently inhibit PI5P4Kγ. The γ-isoform has a very low specific activity, and high enzyme concentration (0.4μM) was used in all assays, which prevented us from obtaining a reliable inhibition curve at low CC260 concentrations. Nevertheless, the compound's K_i could still be calculated fairly accurately to be in the micromolar range (0.8μM), ~20x higher than those obtained for α- and β-isoforms. PI5P4Kγ has a large "gate-keeper" residue (Met-203), whereas PI5P4Kα and PI5P4Kβ both have a threonine there, which may explain the large difference in potency. (**A**) The $K_{m,ATP}$ for PI5P4Kγ was determined to be around 35μM. (**B**) A representative autoradiograph illustrating the extent of inhibition of PI5P4Kγ by 0.8μM or 4μM CC260. (**C**) A comparison of activity inhibition at those two compound concentrations among the three isoforms (all measured in triplicate). The data for PI5P4Kα and PI5P4Kβ were taken from Fig. S9C and S9D.

Figure S11. CC260 potently inhibits PI5P4Kβ-catalyzed reaction using GTP as the phosphodonor. (**A**) and (**B**) GTP has a higher K_m (50μM) but greater V_{max} (2.5 times that of ATP) (12). The titration was performed in triplicate (the ATP titration curve was the same as that in Fig. S9A). (**C**) A representative autoradiograph showing the inhibition of the reaction over a range of CC260 concentrations. In this experiment, GTP concentration was fixed at 50μM (1x K_m).

Figure S12. The crystal structure of PI5P4Kβ. In the co-crystal, the inhibitor is found in only one of the two protomers in the asymmetric unit. (**A**) CC260 caused little conformational change in the kinase, except the Gly-rich loop (apo, black; complex, light orange). Superimposed Cα traces are shown as a cross-eye stereogram. The inhibitor is shown as orange sticks. (**B**) Details of CC260 binding to the lipid kinase. Hydrogen bonds are shown as red dashed lines. (**C**) and (**D**) 2FoFc maps, contoured at 1σ, reveal differences in the conformation of the G-loop between apo and complex structures. The inhibitor is colored in orange.

Figure S13. The selectivity profile of CC260. (**A**) Concentration inhibition curves of CC260 and its parent compounds BI-2536 and BI-D1870 for Plk1- and RSK2-mediated kinase reactions. In both titrations, the ATP concentration was fixed at 50μM. The assay kits for Plk1 and RSK2 were obtained from Promega (Madison, WI), which use ADP-Glo™ for activity detection. (**B**) CC260 did not inhibit PI4P5Kα but showed modest inhibition of PIKfyve. Profiling a panel of 14 lipid kinases at Reaction Biology, which uses

ADP-Glo™ for detecting lipid kinase activities, showed that PI3Kγ and PI3Kδ were also inhibited by CC260 (compound 0.5μM, ATP 10μM). The panel includes PI4P5Kα and another type 1 kinase PI4P5Kγ, neither of which was inhibited (PI4P5Kα 95% activity remaining; PI4P5Kγ 98%). (**C**) CC260 was tested against 396 human protein kinases at Reaction Biology Corporation (Malvern, PA) at a single compound concentration of 0.5μM and an ATP concentration of 20μM using the HotSpot℠ radioisotope filter binding assay. Plk1 and RSK2 are among the kinases examined, and their extent of inhibition (Plk1 activity remaining 97%; RSK2, 83%) is consistent with the results shown in (A) that cover a range of compound concentrations: calculated RSK2 activity at 0.5μM CC260 and 20μM ATP is 79% of that of DMSO control. (**D**) The degree of kinase inhibition at various compound concentrations used in the cell culture experiment assuming an intracellular ATP concentration of 2mM. The $K_{m,ATP}$ value for PIKfyve was based on literature (16).

Figure S14. Measuring intracellular adenine nucleotide concentrations. (**A**) HPLC elution profiles of acid extracts of C2C12 myotubes treated with DMSO or 10μM CC260. (**B**) Quantification of the areas under the ATP peak (measured in triplicate). (**C**) An equimolar mixture of AMP, ADP and ATP standards resolved by LC-MS/MS. (**D**) The fragmentation of AMP or ADP generated PO_3 (theoretical M.W. 79.0 Da), and the fragmentation of ATP yielded a P_2O_6 ion (theoretical M.W. 157.9 Da).

Figure S15. CC260 caused (**A**) AMPK activation (increase of raptor phosphorylation), mTORC1 inhibition (decrease of 4E-BP1 phosphorylation), and (**B**) a small increase of cellular PI(5)P level. BT474 cells were treated with compound overnight in DMEM

medium without serum (n=3). Results are shown as means ± SEM. * indicates $p \leq 0.01$ and *** indicates $p \leq 0.0001$ based on Student's *t*-test.

Figure S16. Overexpression of PI5P4Kα causes AMPK activation. (**A**) Comparing the *in vitro* activities of PI5P4Kα wildtype (WT) and double mutant (DM) at different inhibitor concentrations (n=3). Ile-143 and Thr-196 are equivalent to Val-148 and Thr-201 in PI5P4Kβ. (**B**) and (**C**) Overexpression of PI5P4Kα WT or DM increased ACC phosphorylation. * marks the endogenous lipid kinase (the overexpressed lipid kinases have higher molecular weights due to an N-terminal 3x FLAG tag and linker). In (B), cells were treated with compound (0, 5 and 10μM) overnight in serum-free DMEM medium.

Figure S17. CC260 caused AMPK activation in a panel of breast cancer cells with different p53 status (wildtype, null, missense mutation). (**A**) Cells were treated with 10μM compound overnight in serum-free media before western blot analysis (n=3). BT474 cells harbor a temperature sensitive mutant p53 that regains wildtype function at 32°C (17). (**B**) The relative phosphor-ACC levels are shown as means ± SEM. ** indicates $p \leq 0.001$ and *** indicates $p \leq 0.0001$ based on Student's *t*-test.

Figure S18. PI5P4Kα/β inhibition reduces BT474 cell survival. (**A**) BT474 cells were treated with 10μM CC260 or DMSO in serum-free low-glucose DMEM medium for 18h before being plated (2,000 cells per well) to grow into colonies. The absence of serum during treatment did not significantly reduce the number of colonies (<10%). BT474 cells are not as sensitive to CC260 as MCF-10A cells. (**B**) Heterologous expression of CC260-

refractory PI5P4Kβ mutant, instead of wildtype, rescued cell survival upon compound treatment. The number of colonies were determined by *ImageJ* (n=3). Results are shown as means ± SEM. # indicates $p \leq 0.05$ based on Student's *t*-test.

Figure S19. After overnight CC260 (10μM) treatment or glucose-starvation in serum-free DMEM/F12 medium supplemented with 0.5μg/ml hydrocortisone, 100ng/ml cholera toxin and 10μg/ml insulin, cell death was estimated by LDH activity present in the supernatant (n=3). Results are shown as means ± SEM. *** indicates $p \leq 0.0001$ based on Student's *t*-test. N.S., non-statistically significant.

Figure S20. PI5P4Kα/β inhibition causes oxidative stress in BT474 cells (18). (**A**) CC260 treatment increased ROS and p38 phosphorylation. DCF, dichlorofluorescein; NAC, N-acetyl cysteine. Results are shown as means ± SEM (n=10). *** indicates $p \leq 0.0001$ based on Student's *t*-test. (**B**) The effect of oxidative stress on cell proliferation is time dependent. After a short-term (24 hrs) treatment with CC260 (followed by a 24-hour washout period), the cells resumed growth at a similar rate as untreated cells. Only prolonged treatment produced a lasting effect of cell proliferation. RLU, relative luminescence unit.

Figure S21. Oxygen consumption and medium acidification profiles for (**A**) C2C12 myotubes and (**B**) BT474 cells. OCR, oxygen consumption rate; ECAR, extracellular

acidification rate; Rot, rotenone; AA, antimycin A. Data are presented as means ± SEM of 16 wells.

SI References

1. Muftuoglu Y, Xue Y, Gao X, Wu D, & Ha Y (2016) Mechanism of substrate specificity of phosphatidylinositol phosphate kinases. *Proc Natl Acad Sci U S A* 113(31):8711-8716.
2. Otwinowski Z & Minor W (1997) Processing of X-ray diffraction data collected in oscillation mode. *Methods in enzymology* 276:307-326.
3. Winn MD*, et al.* (2011) Overview of the CCP4 suite and current developments. *Acta crystallographica. Section D, Biological crystallography* 67(Pt 4):235-242.
4. Emsley P, Lohkamp B, Scott WG, & Cowtan K (2010) Features and development of Coot. *Acta crystallographica. Section D, Biological crystallography* 66(Pt 4):486-501.
5. Schuttelkopf AW & van Aalten DM (2004) PRODRG: a tool for high-throughput crystallography of protein-ligand complexes. *Acta crystallographica. Section D, Biological crystallography* 60(Pt 8):1355-1363.
6. Rao VD, Misra S, Boronenkov IV, Anderson RA, & Hurley JH (1998) Structure of type IIbeta phosphatidylinositol phosphate kinase: a protein kinase fold flattened for interfacial phosphorylation. *Cell* 94(6):829-839.
7. Manfredi G, Yang L, Gajewski CD, & Mattiazzi M (2002) Measurements of ATP in mammalian cells. *Methods (San Diego, Calif.)* 26(4):317-326.
8. Schacht J (1978) Purification of polyphosphoinositides by chromatography on immobilized neomycin. *Journal of lipid research* 19(8):1063-1067.
9. Morris JB, Hinchliffe KA, Ciruela A, Letcher AJ, & Irvine RF (2000) Thrombin stimulation of platelets causes an increase in phosphatidylinositol 5-phosphate revealed by mass assay. *FEBS letters* 475(1):57-60.
10. Kunz J, Fuelling A, Kolbe L, & Anderson RA (2002) Stereo-specific substrate recognition by phosphatidylinositol phosphate kinases is swapped by changing a single amino acid residue. *J Biol Chem* 277(7):5611-5619.
11. Liu A, Sui D, Wu D, & Hu J (2016) The activation loop of PIP5K functions as a membrane sensor essential for lipid substrate processing. *Science advances* 2(11):e1600925.
12. Sumita K*, et al.* (2016) The Lipid Kinase PI5P4Kbeta Is an Intracellular GTP Sensor for Metabolism and Tumorigenesis. *Molecular cell* 61(2):187-198.
13. Kothe M*, et al.* (2007) Selectivity-determining residues in Plk1. *Chemical biology & drug design* 70(6):540-546.
14. Demian DJ*, et al.* (2009) High-throughput, cell-free, liposome-based approach for assessing in vitro activity of lipid kinases. *Journal of biomolecular screening* 14(7):838-844.
15. Clarke JH & Irvine RF (2013) Evolutionarily conserved structural changes in phosphatidylinositol 5-phosphate 4-kinase (PI5P4K) isoforms are responsible for differences in enzyme activity and localization. *The Biochemical journal* 454(1):49-57.
16. Fogarty K*, et al.* (2017) Development of Three Orthogonal Assays Suitable for the Identification and Qualification of PIKfyve Inhibitors. *Assay and drug development technologies* 15(5):210-219.
17. Dearth LR*, et al.* (2007) Inactive full-length p53 mutants lacking dominant wild-type p53 inhibition highlight loss of heterozygosity as an important aspect of p53 status in human cancers. *Carcinogenesis* 28(2):289-298.
18. Emerling BM*, et al.* (2013) Depletion of a putatively druggable class of phosphatidylinositol kinases inhibits growth of p53-null tumors. *Cell* 155(4):844-857.

Table S1. Crystallographic statistics for apo and AMP-PNP bound PI5P4Kα (space group: $P6_122$).

Data Collection	Apo	[d]Apo (2)	AMP-PNP	[d]AMP-PNP (2)
Wavelength (Å)	1.075	1.075	1.075	1.075
Unit cell (a, c; Å)	135.7, 95.1	135.7, 94.3	136.1, 95.1	135.9, 94.9
[a]Resolution (Å)	40-2.2 (2.28-2.20)	40-2.5 (2.59-2.50)	40-2.1 (2.18-2.10)	40-2.0 (2.07-2.00)
Redundancy	14.2	18.6	13.6	37.1
Completeness (%)	97.8	100.0	99.7	97.7
$\langle I/\sigma \rangle$	10.8	18.4	11.0	10.3
[a,b]R_{merge}	0.093 (0.870)	0.087 (0.766)	0.074 (0.711)	0.091 (0.726)
Refinement				
Unique reflections	24,766	17,349	29,179	32,904
Number of atoms				
Protein	2,440	2,466	2,468	2,429
Ligand	-	-	33	33
Solvent	168	135	197	205
[c]R_{work}/R_{free}	0.208/0.245	0.197/0.233	0.213/0.251	0.213/0.251
B-factor (Å^2)	54	64	49	52
r.m.s. deviations				
Bond lengths (Å)	0.010	0.007	0.009	0.008
Bond angles (°)	1.225	1.065	1.196	1.165
PDB accession code	7N6Z	7N71	7N7J	7N7K

[a]Highest resolution shell is shown in parentheses.
[b]$R_{merge} = \sum \left| I_i - \langle I \rangle \right| / \sum I_i$
[c]$R_{work} = \sum \left| F_o - F_c \right| / \sum F_o$. R_{free} is the cross-validation R factor for the test set of reflections (5% of the total) omitted in model refinement.
[d]This crystal form, although in the same space group, was obtained from a different crystallization condition.

Table S2. Crystallographic statistics for PI5P4Kα inhibitor complexes (space group: $P6_122$).

Data Collection	BI-D1870	BI-2536	Volasertib	Palbociclib
Wavelength (Å)	1.181	0.979	0.979	0.979
Unit cell (a, c; Å)	136.3, 95.4	136.4, 95.0	136.1, 95.2	135.9, 95.0
[a]Resolution (Å)	40-2.7 (2.80-2.70)	40-2.6 (2.69-2.60)	40-2.3 (2.38-2.30)	40-2.7 (2.80-2.70)
Redundancy	14.2	9.6	14.2	14.4
Completeness (%)	100.0	97.5	100.0	100.0
$\langle I/\sigma \rangle$	10.3	12.0	13.6	10.5
[a,b]R_{merge}	0.149 (0.713)	0.082 (0.827)	0.077 (0.577)	0.074 (0.842)
Refinement				
Unique reflections	14,142	15,422	22,411	14,011
Number of atoms				
Protein	2,366	2,367	2,379	2,377
Ligand	28	38	45	33
Solvent	115	81	135	81
[c]R_{work}/R_{free}	0.193/0.242	0.195/0.236	0.214/0.258	0.197/0.253
B-factor (Å^2)	61	70	61	72
r.m.s. deviations				
Bond lengths (Å)	0.008	0.008	0.007	0.008
Bond angles (°)	1.256	1.228	1.088	1.243
PDB accession code	7N7L	7N7M	7N7N	7N7O

[a]Highest resolution shell is shown in parentheses.
[b]$R_{merge} = \sum \left| I_i - \langle I \rangle \right| / \sum I_i$
[c]$R_{work} = \sum \left| F_o - F_c \right| / \sum F_o$. R_{free} is the cross-validation R factor for the test set of reflections (5% of the total) omitted in model refinement.

Table S3. Crystallographic statistics for PI5P4Kβ (space group: $P2_1$).

Data Collection	Apo	CC260
Wavelength (Å)	0.979	0.979
Cell Dimensions (Å)	a=71.7, b=51.2, c=107.1 β=94.6°	a=73.5, b=51.7, c=107.6 β=95.4°
[a]Resolution (Å)	40-2.5 (2.59-2.50)	40-2.7 (2.80-2.70)
Redundancy	2.6	3.9
Completeness (%)	89.0	98.8
$\langle I/\sigma \rangle$	4.6	7.0
[a,b]R_{merge}	0.129 (0.660)	0.122 (0.968)
Refinement		
Unique reflections	23,433	21,128
Number of Atoms		
Protein	4,588	4,708
Ligand	-	33
Solvent	115	138
[c]R_{work}/R_{free}	0.201/0.283	0.187/0.280
B-factor (Å^2)	61	71
r.m.s. deviations		
Bond lengths (Å)	0.012	0.012
Bond angles (°)	1.645	1.631
PDB accession code	7N80	7N81

[a]Highest resolution shell is shown in parentheses.
[b]$R_{merge} = \sum \left| I_i - \langle I \rangle \right| / \sum I_i$
[c]$R_{work} = \sum \left| F_o - F_c \right| / \sum F_o$. R_{free} is the cross-validation R factor for the test set of reflections (5% of the total) omitted in model refinement.

Table S4.

396 protein kinase panel
CC260 was tested in single dose duplicate mode at a concentration of 0.5μM.
Reactions were carried out at 20μM ATP.

	% Enzyme Activity (relative to DMSO controls)		Average remaining activity %
	CC260		
Kinase:	Data 1	Data 2	
ABL1	92.28	90.87	91.57
ABL2/ARG	99.99	96.86	98.43
ACK1	86.66	85.64	86.15
AKT1	98.84	97.18	98.01
AKT2	90.22	89.64	89.93
AKT3	82.15	81.39	81.77
ALK	105.14	100.99	103.06
ALK1/ACVRL1	123.39	117.89	120.64
ALK2/ACVR1	84.93	84.51	84.72
ALK3/BMPR1A	108.38	102.93	105.66
ALK4/ACVR1B	110.95	110.32	110.64
ALK5/TGFBR1	95.49	93.69	94.59
ALK6/BMPR1B	98.04	91.86	94.95
ARAF	101.50	100.89	101.19
ARK5/NUAK1	93.94	92.80	93.37
ASK1/MAP3K5	95.83	94.74	95.28
Aurora A	96.22	92.20	94.21
Aurora B	89.49	89.14	89.32
Aurora C	103.21	99.47	101.34
AXL	91.32	90.80	91.06
BLK	100.64	100.52	100.58
BMPR2	105.14	105.13	105.14
BMX/ETK	101.29	99.92	100.60
BRAF	107.79	106.20	107.00
BRK	96.97	95.15	96.06
BRSK1	93.45	91.88	92.67
BRSK2	92.24	91.45	91.84
BTK	90.71	88.93	89.82
c-Kit	105.12	104.63	104.87
c-MER	68.84	65.95	67.40
c-MET	99.77	96.30	98.03
c-Src	95.67	95.12	95.40
CAMK1a	97.18	95.72	96.45
CAMK1b	86.06	81.74	83.90
CAMK1d	93.71	91.08	92.39
CAMK1g	93.55	93.42	93.48
CAMK2a	116.44	108.25	112.35
CAMK2b	95.55	95.11	95.33
CAMK2d	108.14	106.50	107.32
CAMK2g	94.20	92.44	93.32
CAMK4	99.57	98.26	98.92
CAMKK1	93.43	89.74	91.59
CAMKK2	83.33	82.74	83.04

17 lipid kinase panel
CC260 was tested in single dose duplicate mode at 0.5μM.
Reactions were carried out at 10 μM ATP.

		% Enzyme Activity (relative to DMSO controls)		Average remaining activity %
		CC260		
Kinase:	Substrate:	Data 1	Data 2	
PI3KC2A	Phosphatidylinositol	89.53	89.37	89.45
PI3KC3	PI:PS	101.42	100.84	101.13
PI4Ka	Phosphatidylinositol	110.06	111.42	110.74
PI4Kb	Phosphatidylinositol	88.83	88.54	88.69
PI4K2A	Phosphatidylinositol	93.00	94.59	93.80
PIP5K1A	PI(4)P:PS	95.61	95.27	95.44
PIP5K1C	PI(4)P:PS	97.83	97.99	97.91
SPHK1	Sphingosine	96.86	95.83	96.35
SPHK2	Sphingosine	111.21	110.51	110.86
PI3Ka (p110a/p85a)	PI(4,5)P2:PS	94.36	93.70	94.03
PI3Kb (p110b/p85a)	PI(4,5)P2:PS	118.22	117.07	117.65
PI3Kg (p110g)	PI(4,5)P2:PS	57.77	55.89	56.83
PI3Kd (p110d/p85a)	PI(4,5)P2:PS	20.81	19.36	20.08
PI3K (p110a/p65a)	PI(4,5)P2:PS	106.44	106.53	106.49
PI3K (p110a(E542K)/p85a)	PI(4,5)P2:PS	107.17	107.12	107.15
PI3K (p110a(E545K)/p85a)	PI(4,5)P2:PS	107.58	107.41	107.49
PI3K (p110a(H1047R)/p85a)	PI(4,5)P2:PS	98.47	100.80	99.64

CDC7/DBF4	97.83	93.73	95.78
CDK1/cyclin A	99.56	99.46	99.51
CDK1/cyclin B	105.10	104.19	104.64
CDK1/cyclin E	99.37	99.12	99.25
CDK14/cyclin Y (PFTK1)	100.95	100.56	100.76
CDK16/cyclin Y (PCTAIRE)	104.02	103.33	103.68
CDK17/cyclin Y (PCTK2)	98.29	97.97	98.13
CDK18/cyclin Y (PCTK3)	92.53	87.80	90.16
CDK19/cyclin C	95.23	93.14	94.18
CDK2/cyclin A	94.93	93.78	94.35
CDK2/Cyclin A1	104.15	102.73	103.44
CDK2/cyclin E	99.03	97.49	98.26
CDK2/cyclin E2	98.87	98.16	98.51
CDK2/cyclin O	105.79	105.45	105.62
CDK20/cyclin H	101.58	100.65	101.11
CDK20/cyclin T1	98.65	96.65	97.65
CDK3/cyclin E	97.43	95.53	96.48
CDK3/cyclin E2	88.07	87.93	88.00
CDK4/cyclin D1	101.94	98.02	99.98
CDK4/cyclin D3	106.03	104.74	105.38
CDK5/p25	107.16	104.83	106.00
CDK5/p35	98.99	96.57	97.78
CDK6/cyclin D1	100.54	99.28	99.91
CDK6/cyclin D3	102.30	101.27	101.79
CDK7/cyclin H	99.89	99.25	99.57
CDK8/cyclin C	96.29	96.13	96.21
CDK9/cyclin K	102.73	98.06	100.39
CDK9/cyclin T1	95.16	94.87	95.01
CDK9/cyclin T2	105.86	101.78	103.82
CHK1	106.55	101.16	103.85
CHK2	100.19	99.56	99.87
CK1a1	95.08	91.91	93.50
CK1a1L	105.32	104.61	104.96
CK1d	111.46	103.65	107.56
CK1epsilon	97.80	96.57	97.19
CK1g1	94.54	94.47	94.50
CK1g2	96.08	95.43	95.76
CK1g3	109.12	106.46	107.79
CK2a	104.25	103.00	103.62
CK2a2	89.36	88.21	88.78
CLK1	80.95	80.30	80.62
CLK2	119.29	115.41	117.35
CLK3	101.41	94.01	97.71
CLK4	92.15	87.02	89.59
COT1/MAP3K8	91.95	90.57	91.26
CSK	98.60	98.08	98.34
CTK/MATK	108.66	106.87	107.76
DAPK1	79.00	77.65	78.33
DAPK2	106.10	103.19	104.65
DCAMKL1	114.97	110.00	112.49
DCAMKL2	97.04	95.96	96.50
DDR1	101.68	101.29	101.49
DDR2	112.44	108.77	110.60

DLK/MAP3K12	110.56	107.05	108.80
DMPK	105.49	105.26	105.38
DMPK2	103.65	102.14	102.90
DRAK1/STK17A	103.88	103.73	103.80
DYRK1/DYRK1A	95.00	94.68	94.84
DYRK1B	96.77	95.84	96.30
DYRK2	100.92	98.45	99.69
DYRK3	111.12	110.13	110.63
DYRK4	103.07	99.66	101.36
EGFR	89.30	88.93	89.12
EPHA1	93.24	93.09	93.16
EPHA2	94.36	92.84	93.60
EPHA3	87.41	84.29	85.85
EPHA4	93.53	90.69	92.11
EPHA5	101.30	100.90	101.10
EPHA6	105.63	100.24	102.93
EPHA7	92.33	91.12	91.73
EPHA8	100.06	100.05	100.05
EPHB1	91.31	90.62	90.97
EPHB2	96.19	95.00	95.59
EPHB3	102.15	101.09	101.62
EPHB4	106.70	106.12	106.41
ERBB2/HER2	107.34	107.02	107.18
ERBB4/HER4	87.52	86.40	86.96
ERK1	111.75	109.11	110.43
ERK2/MAPK1	108.84	100.47	104.65
ERK5/MAPK7	92.77	92.29	92.53
ERK7/MAPK15	108.37	107.38	107.87
ERN1/IRE1	94.97	92.50	93.73
ERN2/IRE2	102.91	96.46	99.68
FAK/PTK2	97.23	96.30	96.76
FER	91.72	86.81	89.26
FES/FPS	104.43	103.51	103.97
FGFR1	97.87	96.77	97.32
FGFR2	117.13	113.29	115.21
FGFR3	100.51	99.37	99.94
FGFR4	100.71	100.49	100.60
FGR	81.97	81.03	81.50
FLT1/VEGFR1	101.59	99.18	100.39
FLT3	85.14	84.70	84.92
FLT4/VEGFR3	134.23	128.42	131.32
FMS	96.77	96.53	96.65
FRK/PTK5	97.32	96.72	97.02
FYN	107.51	106.39	106.95
GCK/MAP4K2	88.80	88.77	88.79
GLK/MAP4K3	104.37	103.78	104.08
GRK1	121.06	114.37	117.72
GRK2	97.34	96.89	97.11
GRK3	110.15	107.46	108.81
GRK4	100.77	100.45	100.61
GRK5	92.54	92.39	92.47
GRK6	106.88	106.45	106.66
GRK7	108.71	102.97	105.84

GSK3a	97.71	94.60	96.15
GSK3b	113.41	111.80	112.60
Haspin	103.12	102.12	102.62
HCK	92.86	89.92	91.39
HGK/MAP4K4	89.92	87.07	88.50
HIPK1	121.67	119.30	120.48
HIPK2	93.29	91.95	92.62
HIPK3	99.41	94.72	97.07
HIPK4	109.73	108.97	109.35
HPK1/MAP4K1	130.23	128.46	129.34
IGF1R	101.29	98.80	100.04
IKKa/CHUK	93.43	87.95	90.69
IKKb/IKBKB	108.24	104.26	106.25
IKKe/IKBKE	106.72	103.00	104.86
IR	106.40	104.48	105.44
IRAK1	98.28	95.72	97.00
IRAK4	113.26	110.86	112.06
IRR/INSRR	84.80	83.69	84.25
ITK	82.36	80.37	81.37
JAK1	112.51	110.47	111.49
JAK2	100.58	100.20	100.39
JAK3	106.88	104.87	105.87
JNK1	97.16	97.02	97.09
JNK2	108.23	105.70	106.97
JNK3	90.45	89.61	90.03
KDR/VEGFR2	84.43	83.47	83.95
KHS/MAP4K5	83.29	82.55	82.92
KSR1	121.03	116.95	118.99
KSR2	100.61	99.97	100.29
LATS1	98.31	97.53	97.92
LATS2	96.25	95.37	95.81
LCK	95.14	94.62	94.88
LCK2/ICK	119.72	107.77	113.74
LIMK1	89.80	88.37	89.08
LIMK2	137.87	136.34	137.10
LKB1	96.63	95.81	96.22
LOK/STK10	108.92	107.06	107.99
LRRK2	94.02	93.45	93.74
LYN	112.28	111.61	111.95
LYN B	105.25	104.46	104.85
MAK	96.14	95.72	95.93
MAPKAPK2	94.09	92.26	93.18
MAPKAPK3	94.79	92.43	93.61
MAPKAPK5/PRAK	105.29	100.01	102.65
MARK1	95.20	92.40	93.80
MARK2/PAR-1Ba	95.00	92.20	93.60
MARK3	92.64	89.91	91.27
MARK4	104.70	103.88	104.29
MASTL	94.27	94.08	94.18
MEK1	106.40	102.35	104.37
MEK2	95.62	94.74	95.18
MEK3	104.40	101.01	102.71
MEK5	106.93	105.93	106.43

MEKK1	116.82	110.21	113.52
MEKK2	119.74	118.60	119.17
MEKK3	106.07	99.78	102.92
MEKK6	110.98	107.39	109.19
MELK	97.09	95.96	96.53
MINK/MINK1	104.54	103.09	103.82
MKK4	103.01	98.68	100.85
MKK6	98.85	97.42	98.14
MKK7	103.64	103.47	103.55
MLCK/MYLK	96.85	95.78	96.31
MLCK2/MYLK2	109.78	108.59	109.18
MLK1/MAP3K9	100.38	98.84	99.61
MLK2/MAP3K10	105.78	102.01	103.90
MLK3/MAP3K11	83.79	83.13	83.46
MLK4	103.22	102.03	102.62
MNK1	83.04	80.06	81.55
MNK2	98.18	91.53	94.86
MRCKa/CDC42BPA	112.79	111.59	112.19
MRCKb/CDC42BPB	105.42	105.21	105.32
MSK1/RPS6KA5	101.36	99.93	100.64
MSK2/RPS6KA4	93.47	91.90	92.69
MSSK1/STK23	99.80	97.39	98.59
MST1/STK4	97.03	96.33	96.68
MST2/STK3	91.53	87.88	89.71
MST3/STK24	90.79	89.79	90.29
MST4	94.91	94.17	94.54
MUSK	91.08	89.44	90.26
MYLK3	101.16	100.94	101.05
MYLK4	108.41	104.98	106.70
MYO3A	96.20	96.13	96.16
MYO3b	110.53	105.64	108.09
NEK1	66.74	66.26	66.50
NEK11	67.36	65.63	66.50
NEK2	112.14	111.81	111.98
NEK3	96.38	95.32	95.85
NEK4	98.17	96.05	97.11
NEK5	95.80	93.70	94.75
NEK6	97.76	94.71	96.24
NEK7	96.68	94.21	95.44
NEK8	87.82	86.84	87.33
NEK9	83.65	82.94	83.29
NIM1	110.65	107.61	109.13
NLK	109.18	105.22	107.20
OSR1/OXSR1	99.28	98.02	98.65
P38a/MAPK14	99.85	97.95	98.90
P38b/MAPK11	103.15	99.48	101.32
P38d/MAPK13	101.22	100.85	101.03
P38g	93.23	92.29	92.76
p70S6K/RPS6KB1	100.41	99.37	99.89
p70S6Kb/RPS6KB2	98.38	90.97	94.67
PAK1	92.87	92.34	92.60
PAK2	98.46	96.30	97.38
PAK3	99.69	98.90	99.29

PAK4	108.70	103.59	106.14
PAK5	111.68	108.33	110.01
PAK6	95.33	94.84	95.09
PASK	105.11	104.62	104.87
PBK/TOPK	123.21	120.43	121.82
PDGFRa	102.13	99.40	100.77
PDGFRb	97.30	94.87	96.09
PDK1/PDPK1	93.52	90.32	91.92
PEAK1	83.66	83.13	83.39
PHKg1	93.05	90.72	91.89
PHKg2	101.20	94.82	98.01
PIM1	93.11	91.76	92.43
PIM2	94.95	90.96	92.95
PIM3	94.63	94.52	94.58
PKA	91.70	89.69	90.70
PKAcb	105.55	103.46	104.50
PKAcg	103.78	102.91	103.35
PKCa	102.78	102.67	102.72
PKCb1	92.92	92.23	92.57
PKCb2	99.19	98.60	98.89
PKCd	98.90	97.67	98.29
PKCepsilon	105.57	104.17	104.87
PKCeta	102.51	102.14	102.32
PKCg	96.67	96.06	96.36
PKCiota	99.84	98.37	99.11
PKCmu/PRKD1	101.96	99.32	100.64
PKCnu/PRKD3	95.54	92.08	93.81
PKCtheta	89.69	89.26	89.48
PKCzeta	106.94	105.13	106.03
PKD2/PRKD2	102.44	99.83	101.13
PKG1a	91.83	91.61	91.72
PKG1b	93.61	93.47	93.54
PKG2/PRKG2	110.94	104.44	107.69
PKMYT1	96.07	92.85	94.46
PKN1/PRK1	95.18	92.84	94.01
PKN2/PRK2	93.67	92.52	93.09
PKN3/PRK3	94.87	90.36	92.61
PLK1	97.76	97.06	97.41
PLK2	75.49	74.11	74.80
PLK3	105.84	105.77	105.80
PLK4/SAK	89.65	85.32	87.48
PRKX	91.28	85.97	88.62
PYK2	102.32	101.85	102.09
RAF1	100.43	99.46	99.94
RET	94.09	93.55	93.82
RIPK2	109.75	109.39	109.57
RIPK3	112.77	111.93	112.35
RIPK4	100.79	100.00	100.40
RIPK5	99.21	99.01	99.11
ROCK1	106.57	104.34	105.45
ROCK2	109.13	106.84	107.99
RON/MST1R	101.39	101.16	101.28
ROS/ROS1	92.14	91.87	92.00

RSK1	88.75	86.83	87.79
RSK2	83.56	81.87	82.71
RSK3	113.38	109.97	111.68
RSK4	91.21	90.28	90.75
SBK1	99.90	99.87	99.89
SGK1	95.44	94.44	94.94
SGK2	90.17	87.21	88.69
SGK3/SGKL	103.41	97.64	100.53
SIK1	92.77	91.71	92.24
SIK2	101.27	100.66	100.97
SIK3	112.28	110.45	111.37
SLK/STK2	97.18	96.88	97.03
SNARK/NUAK2	105.86	103.91	104.88
SNRK	84.67	84.64	84.65
SRMS	92.32	90.84	91.58
SRPK1	97.97	96.22	97.09
SRPK2	92.48	92.45	92.47
SSTK/TSSK6	97.46	96.80	97.13
STK16	111.28	110.69	110.98
STK21/CIT	117.07	114.50	115.78
STK22D/TSSK1	95.53	94.31	94.92
STK25/YSK1	87.15	86.47	86.81
STK32B/YANK2	101.61	100.44	101.02
STK32C/YANK3	97.19	96.92	97.06
STK33	86.52	82.53	84.52
STK38/NDR1	94.39	93.50	93.95
STK38L/NDR2	97.96	97.86	97.91
STK39/STLK3	99.54	98.59	99.07
SYK	104.76	104.12	104.44
TAK1	102.72	102.49	102.60
TAOK1	105.73	105.48	105.61
TAOK2/TAO1	85.71	84.93	85.32
TAOK3/JIK	103.03	101.70	102.36
TBK1	98.49	98.26	98.37
TEC	121.23	119.94	120.59
TESK1	86.34	86.09	86.21
TESK2	98.08	95.39	96.74
TGFBR2	89.32	86.82	88.07
TIE2/TEK	81.08	79.82	80.45
TLK1	98.79	96.94	97.87
TLK2	122.29	120.35	121.32
TNIK	73.17	72.09	72.63
TNK1	100.53	97.42	98.97
TRKA	92.53	91.97	92.25
TRKB	88.78	81.51	85.15
TRKC	98.99	94.55	96.77
TSSK2	111.19	110.54	110.86
TSSK3/STK22C	108.30	105.94	107.12
TTBK1	92.96	89.41	91.18
TTBK2	106.34	106.04	106.19
TXK	90.39	90.01	90.20
TYK1/LTK	99.00	98.65	98.83
TYK2	100.95	99.70	100.32

TYRO3/SKY	72.37	70.71	71.54
ULK1	100.31	98.78	99.55
ULK2	98.30	95.66	96.98
ULK3	111.03	103.67	107.35
VRK1	93.80	92.41	93.11
VRK2	101.80	98.92	100.36
WEE1	111.39	105.50	108.45
WNK1	102.78	102.61	102.69
WNK2	106.80	103.65	105.22
WNK3	97.42	93.81	95.62
YES/YES1	100.22	96.64	98.43
YSK4/MAP3K19	99.13	98.83	98.98
ZAK/MLTK	92.91	92.83	92.87
ZAP70	118.14	112.71	115.43
ZIPK/DAPK3	94.26	94.19	94.23
AMPK(A1/B1/G1)	110.52	110.07	110.30
AMPK(A1/B1/G2)	101.07	98.19	99.63
AMPK(A1/B1/G3)	109.60	109.43	109.51
AMPK(A1/B2/G1)	109.93	108.57	109.25
AMPK(A2/B1/G1)	115.93	108.57	112.25
AMPK(A2/B2/G1)	105.07	101.79	103.43
AMPK(A2/B2/G2)	109.53	108.89	109.21
AMPK(A2/B2/G3)	95.47	93.04	94.25
DNA-PK	109.13	101.72	105.42
EEF2K	98.91	94.28	96.60
EIF2AK1	113.62	109.36	111.49
EIF2AK2	102.00	101.11	101.55
EIF2AK3	49.56	47.08	48.32
EIF2AK4	91.71	90.66	91.18
mTOR/FRAP1	105.19	94.65	99.92
PDK1/PDHK1	100.97	100.26	100.62
PDK2/PDHK2	106.85	101.49	104.17
PDK3/PDHK3	104.20	102.96	103.58
PDK4/PDHK4	89.98	89.83	89.91
TRPM7/CHAK1	145.94	144.73	145.34

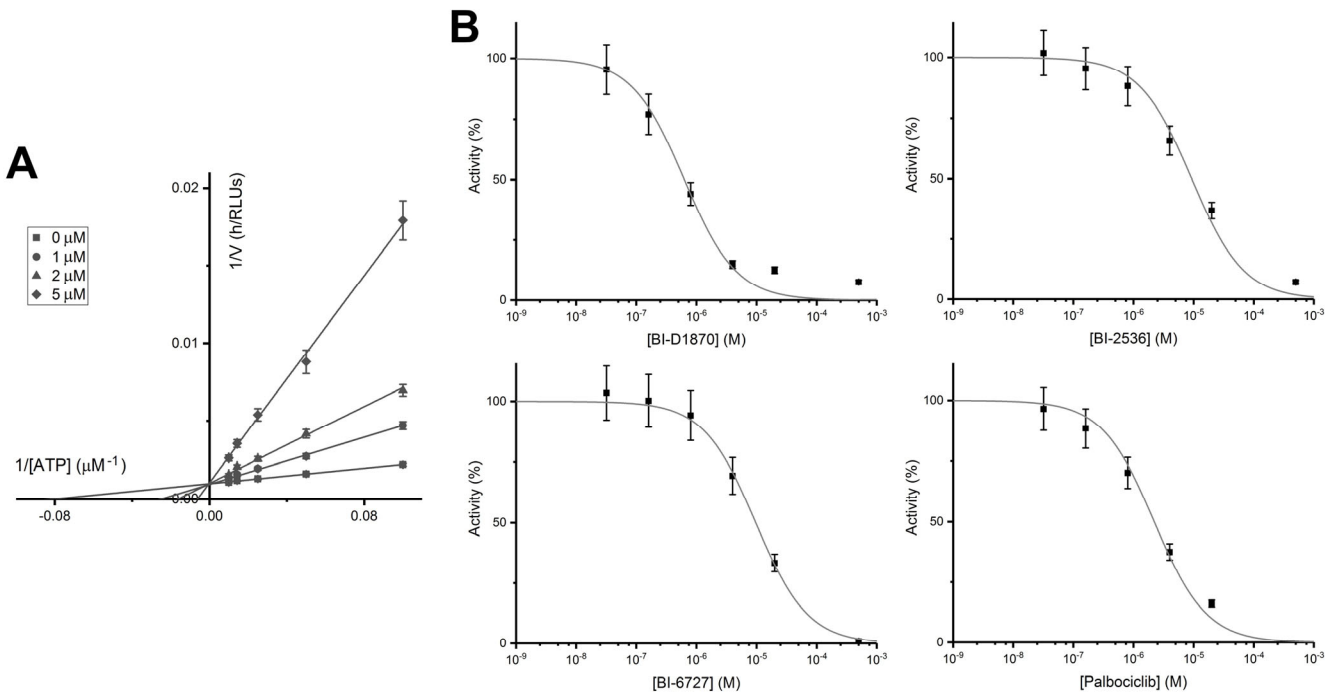
A
0 µM
1 µM
2 µM
5 µM
1/V (h/RLUs)
1/[ATP] (µM-1)
0.02
0.01
0.00
-0.08
0.00
0.08
B
Activity (%)
[BI-D1870] (M)
[BI-2536] (M)
[BI-6727] (M)
[Palbociclib] (M)

Figure S1

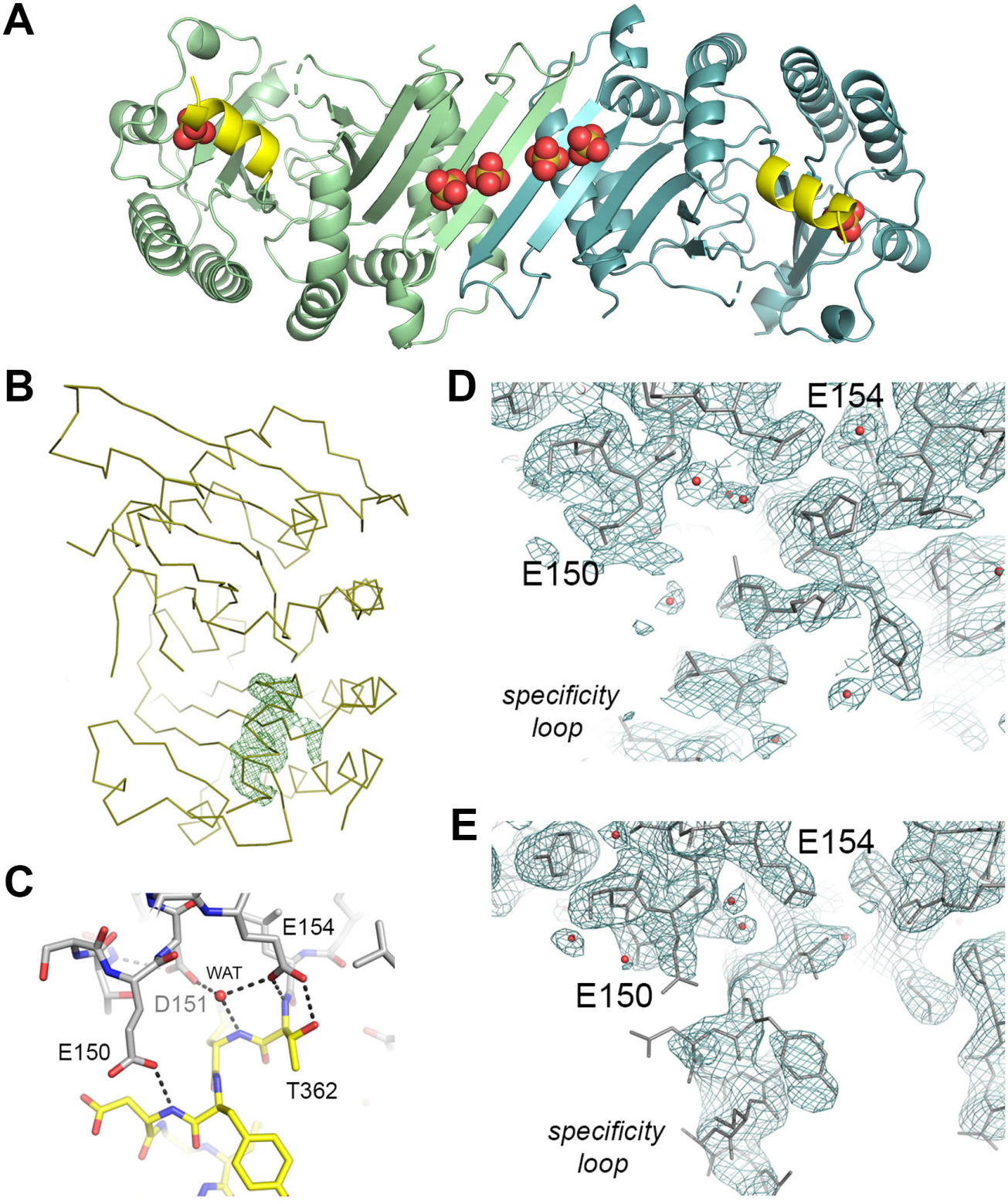
A
B
C
D
E
E154
E150
specificity
loop
E154
WAT
D151
E150
T362
E154
E150
specificity
loop

Figure S2

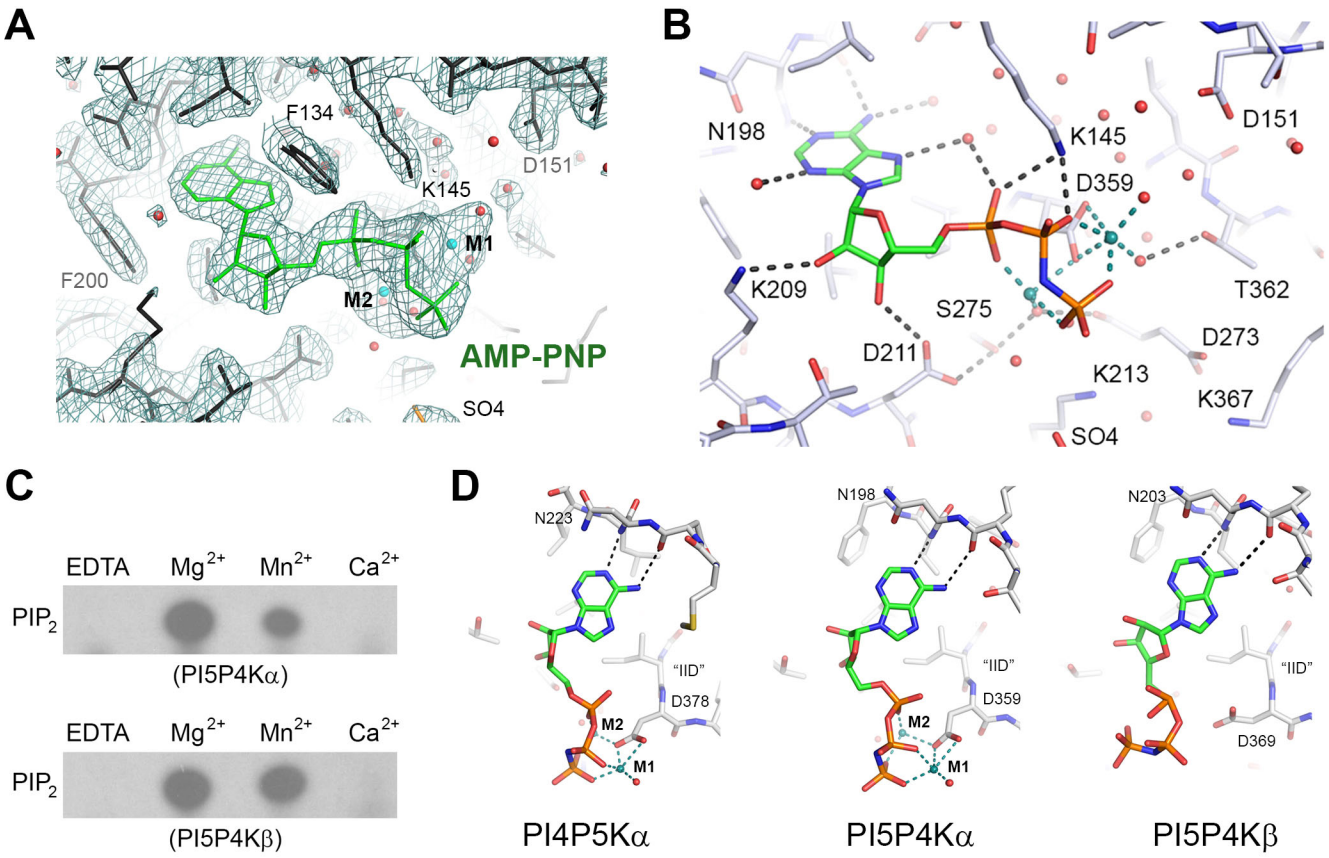
A
F134
D151
K145
M1
F200
M2
AMP-PNP
SO4
B
N198
K145
D151
D359
K209
S275
T362
D273
D211
K213
K367
SO4
C
EDTA
Mg2+
Mn2+
Ca2+
PIP2
(PI5P4Kα)
EDTA
Mg2+
Mn2+
Ca2+
PIP2
(PI5P4Kβ)
D
N223
"IID"
D378
M2
M1
PI4P5Kα
N198
"IID"
D359
M2
M1
PI5P4Kα
N203
"IID"
D369
PI5P4Kβ

Figure S3

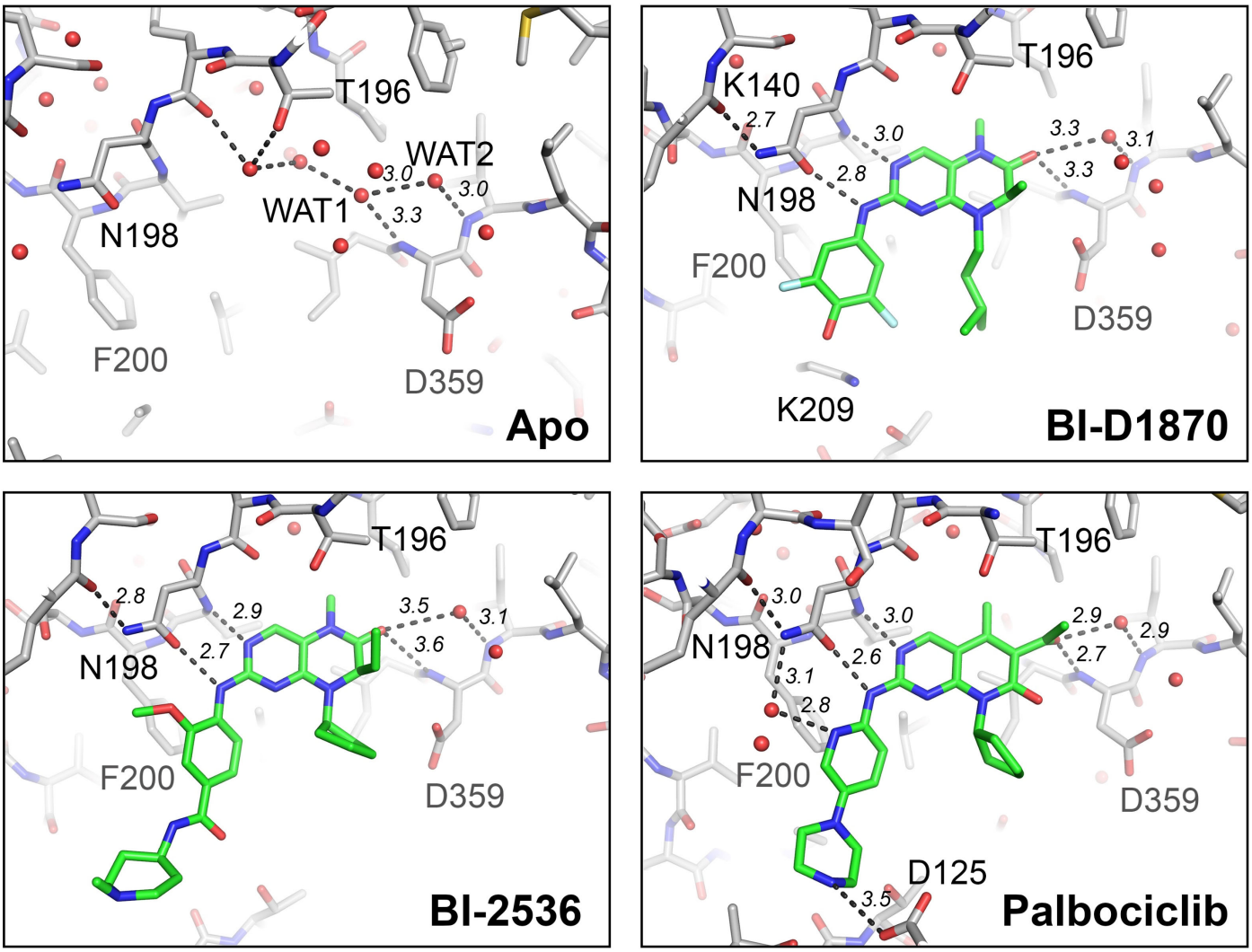
T196
WAT2
WAT1
N198
F200
D359
Apo
T196
K140
N198
F200
D359
K209
BI-D1870
T196
N198
F200
D359
BI-2536
T196
N198
F200
D359
D125
Palbociclib

Figure S4

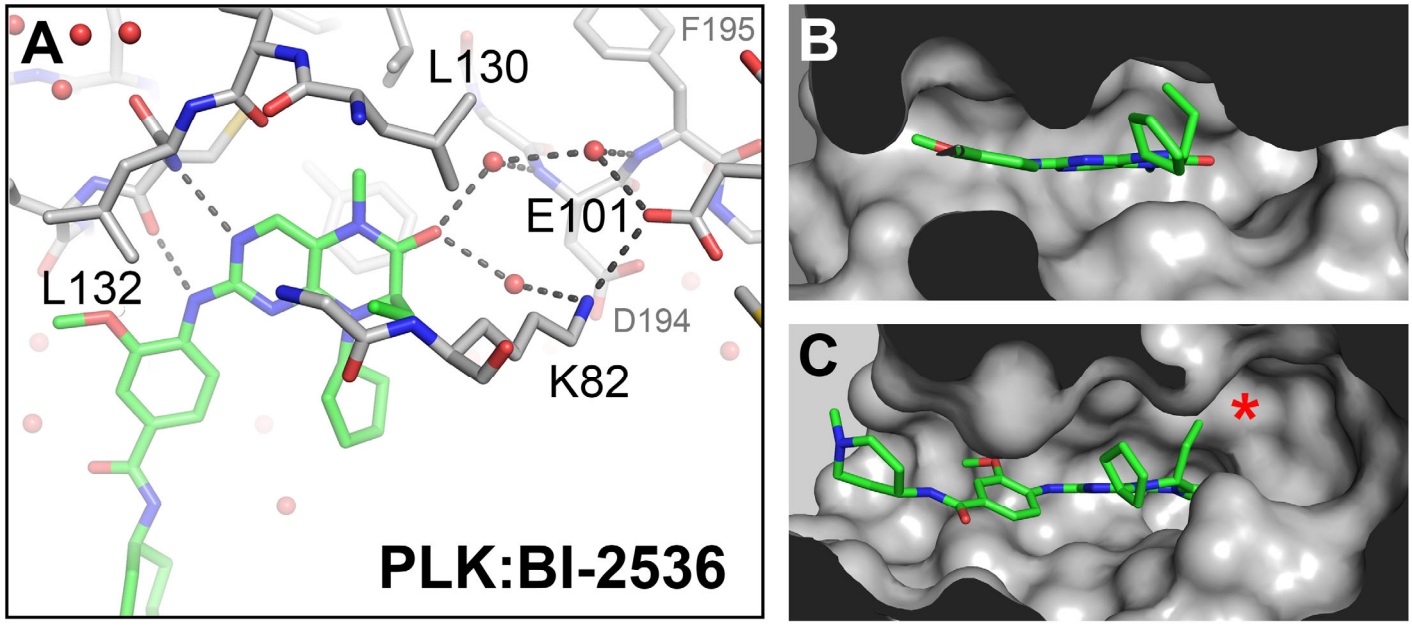

Figure S5

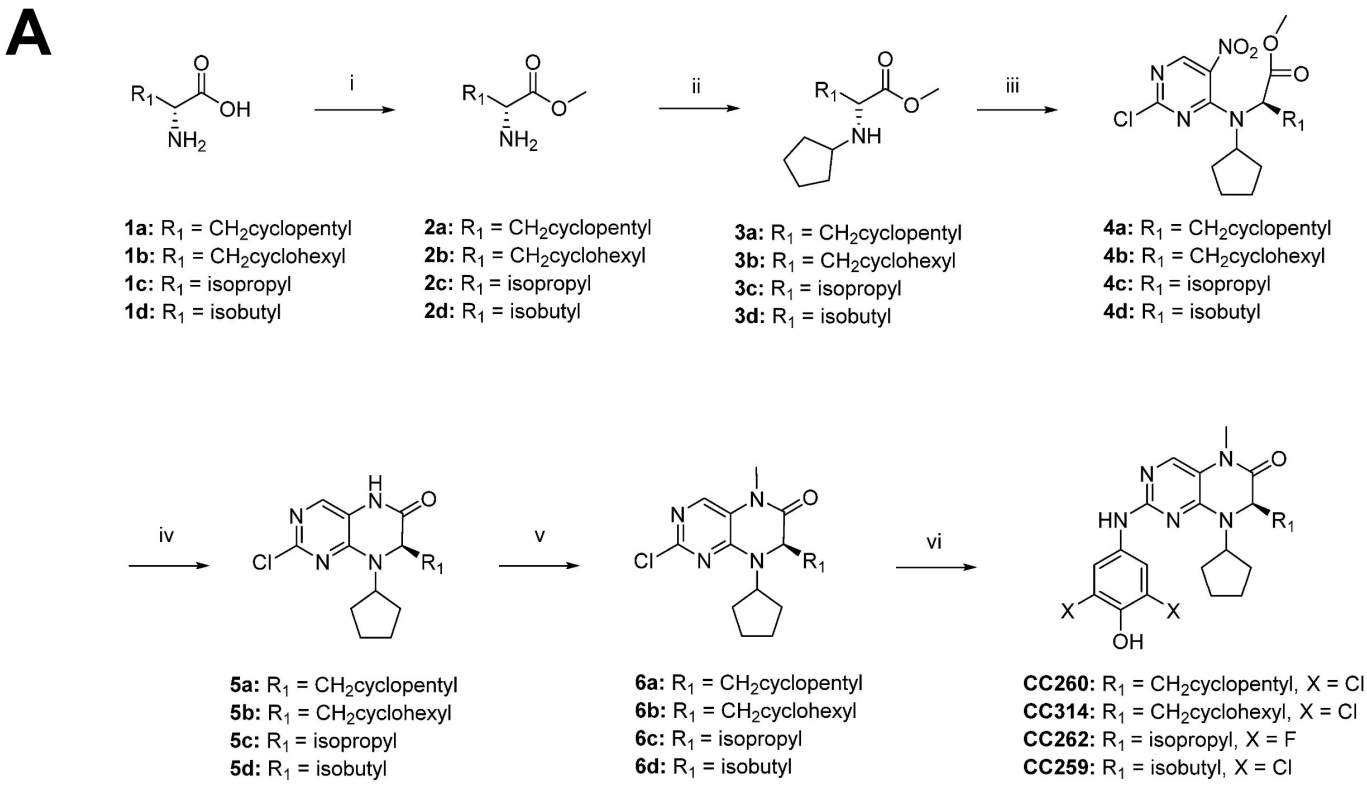
A
i
ii
iii
iv
v
vi
1a: R1 = CH2cyclopentyl
1b: R1 = CH2cyclohexyl
1c: R1 = isopropyl
1d: R1 = isobutyl
2a: R1 = CH2cyclopentyl
2b: R1 = CH2cyclohexyl
2c: R1 = isopropyl
2d: R1 = isobutyl
3a: R1 = CH2cyclopentyl
3b: R1 = CH2cyclohexyl
3c: R1 = isopropyl
3d: R1 = isobutyl
4a: R1 = CH2cyclopentyl
4b: R1 = CH2cyclohexyl
4c: R1 = isopropyl
4d: R1 = isobutyl
5a: R1 = CH2cyclopentyl
5b: R1 = CH2cyclohexyl
5c: R1 = isopropyl
5d: R1 = isobutyl
6a: R1 = CH2cyclopentyl
6b: R1 = CH2cyclohexyl
6c: R1 = isopropyl
6d: R1 = isobutyl
CC260: R1 = CH2cyclopentyl, X = Cl
CC314: R1 = CH2cyclohexyl, X = Cl
CC262: R1 = isopropyl, X = F
CC259: R1 = isobutyl, X = Cl

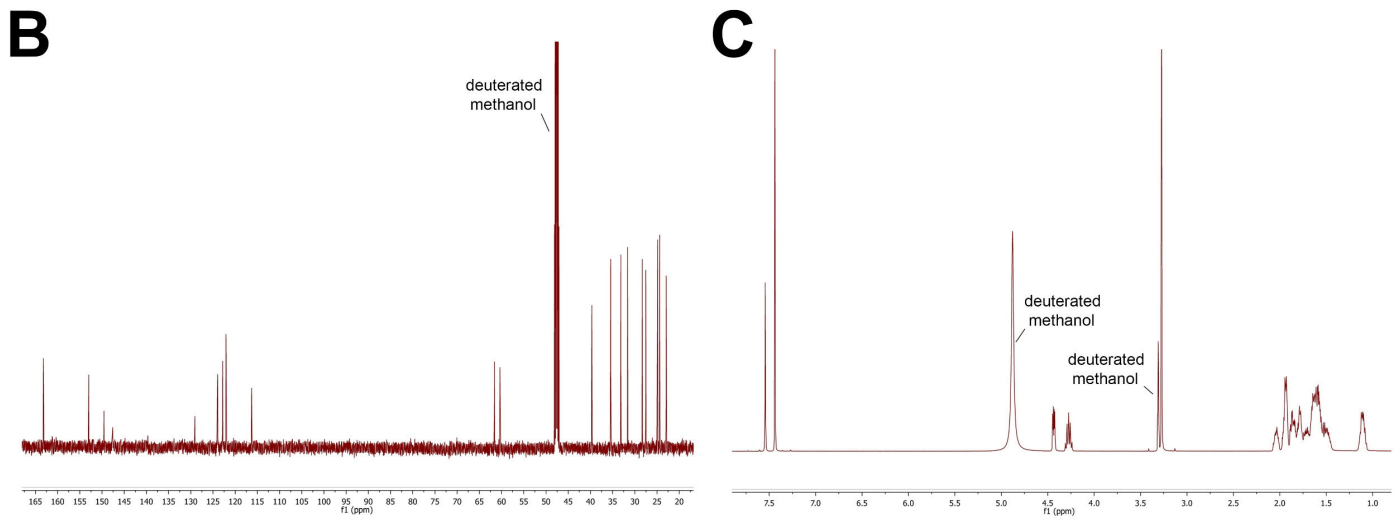
B
deuterated methanol
f1 (ppm)
C
deuterated methanol
deuterated methanol
f1 (ppm)

Figure S6

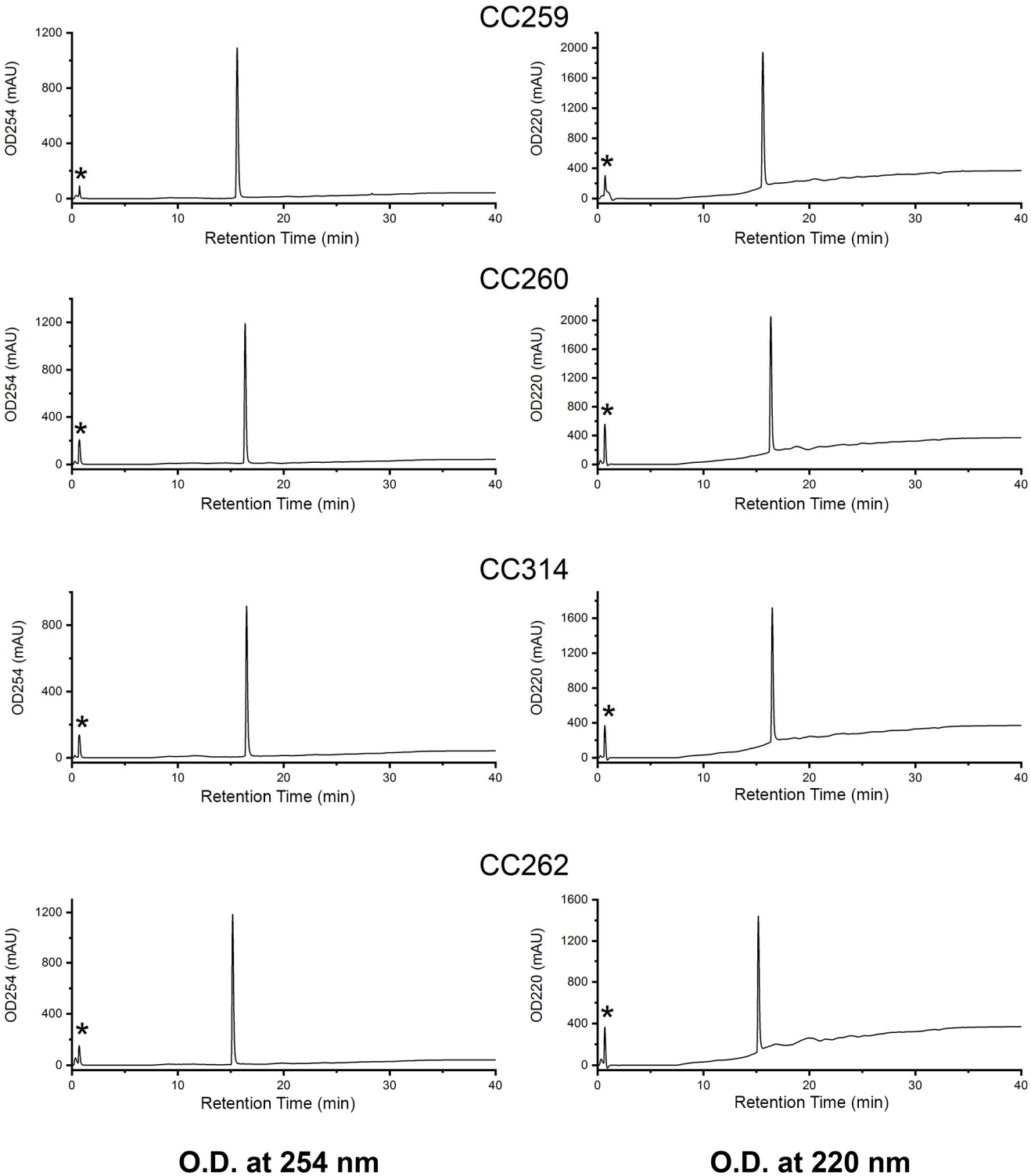
CC259
CC260
CC314
CC262
OD254 (mAU)
OD220 (mAU)
Retention Time (min)
*
O.D. at 254 nm
O.D. at 220 nm

Figure S7

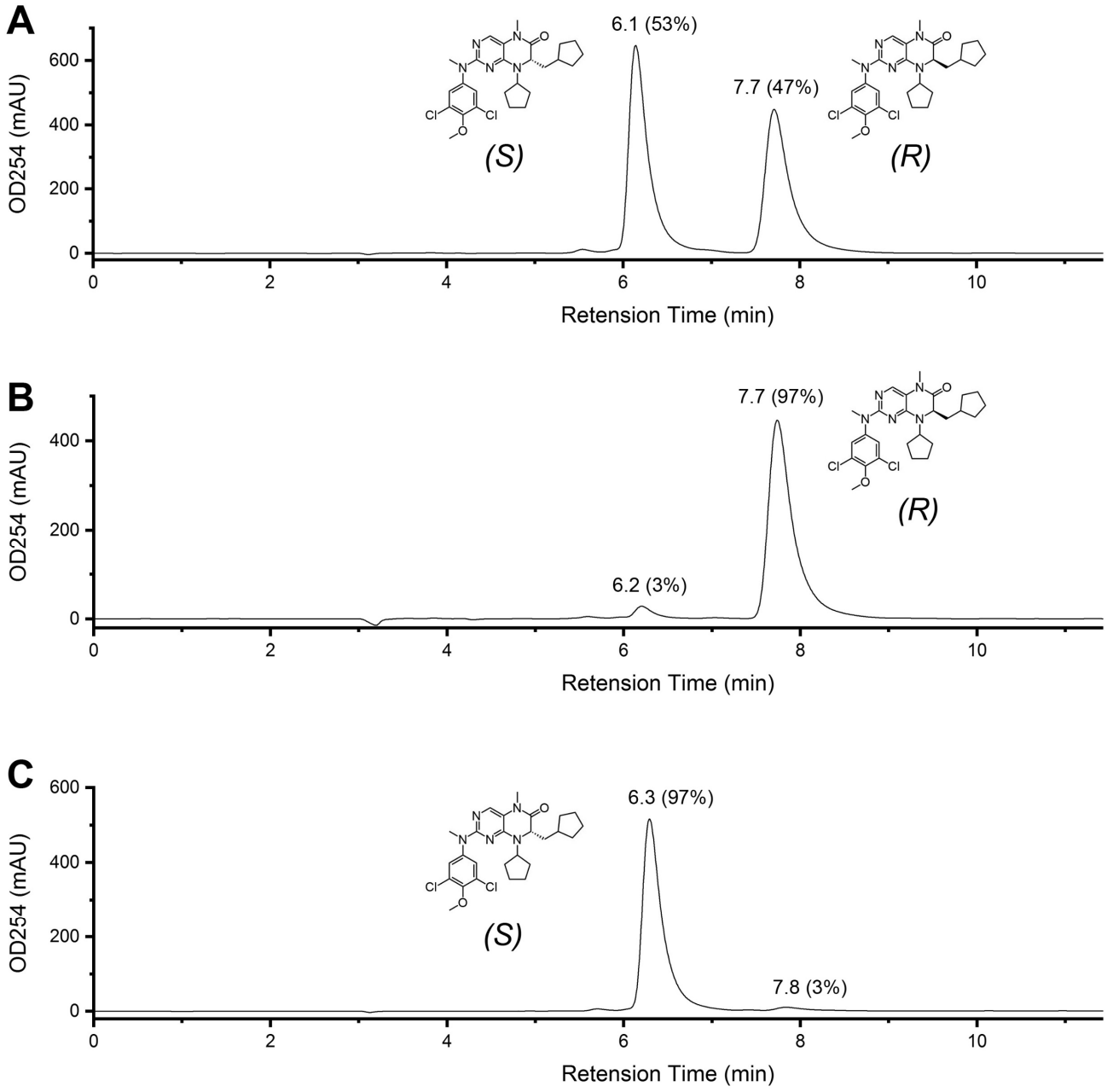
A
6.1 (53%)
7.7 (47%)
(S)
(R)
OD254 (mAU)
Retension Time (min)
B
7.7 (97%)
(R)
6.2 (3%)
OD254 (mAU)
Retension Time (min)
C
6.3 (97%)
(S)
7.8 (3%)
OD254 (mAU)
Retension Time (min)

Figure S8

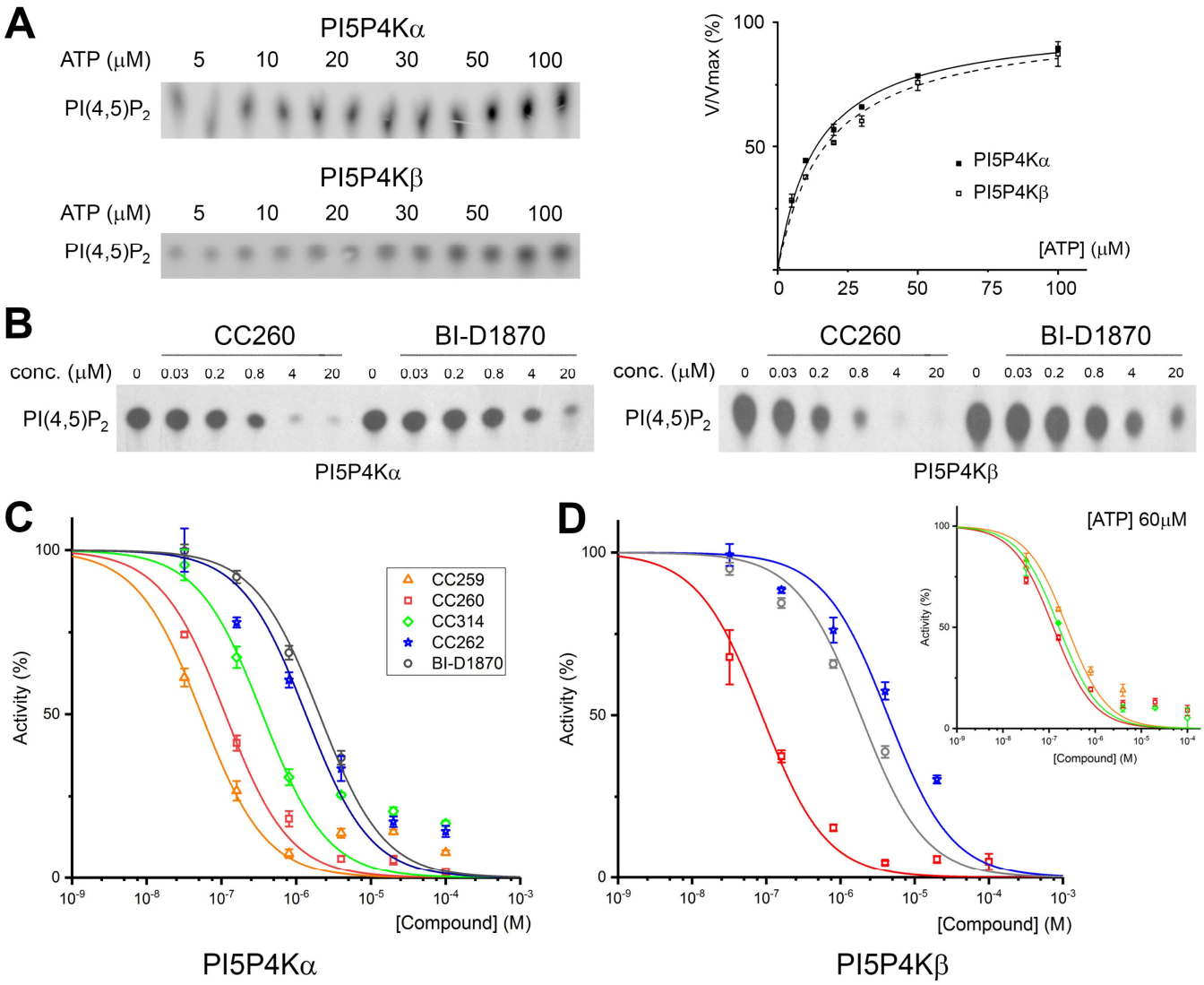
A
PI5P4Kα
ATP (μM) 5 10 20 30 50 100
PI(4,5)P2
PI5P4Kβ
ATP (μM) 5 10 20 30 50 100
PI(4,5)P2
V/Vmax (%)
100
50
PI5P4Kα
PI5P4Kβ
[ATP] (μM)
0 25 50 75 100
B
CC260
BI-D1870
conc. (μM) 0 0.03 0.2 0.8 4 20 0 0.03 0.2 0.8 4 20
PI(4,5)P2
PI5P4Kα
CC260
BI-D1870
conc. (μM) 0 0.03 0.2 0.8 4 20 0 0.03 0.2 0.8 4 20
PI(4,5)P2
PI5P4Kβ
C
Activity (%)
100
50
0
CC259
CC260
CC314
CC262
BI-D1870
10-9 10-8 10-7 10-6 10-5 10-4 10-3
[Compound] (M)
PI5P4Kα
D
Activity (%)
100
50
0
[ATP] 60μM
Activity (%)
100
50
0
10-9 10-8 10-7 10-6 10-5 10-4
[Compound] (M)
10-9 10-8 10-7 10-6 10-5 10-4 10-3
[Compound] (M)
PI5P4Kβ

Figure S9

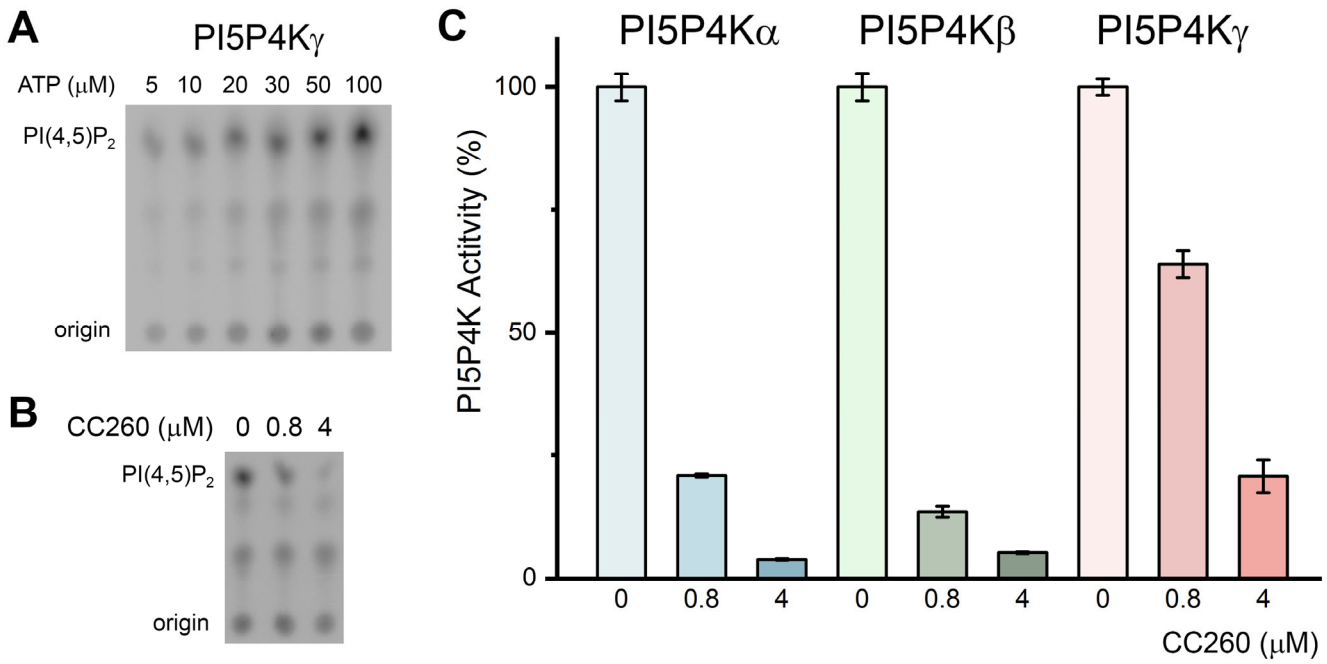
A
PI5P4Kγ
ATP (μM) 5 10 20 30 50 100
PI(4,5)P2
origin
B
CC260 (μM) 0 0.8 4
PI(4,5)P2
origin
C
PI5P4Kα
PI5P4Kβ
PI5P4Kγ
PI5P4K Activity (%)
100
50
0
0 0.8 4 0 0.8 4 0 0.8 4
CC260 (μM)

Figure S10

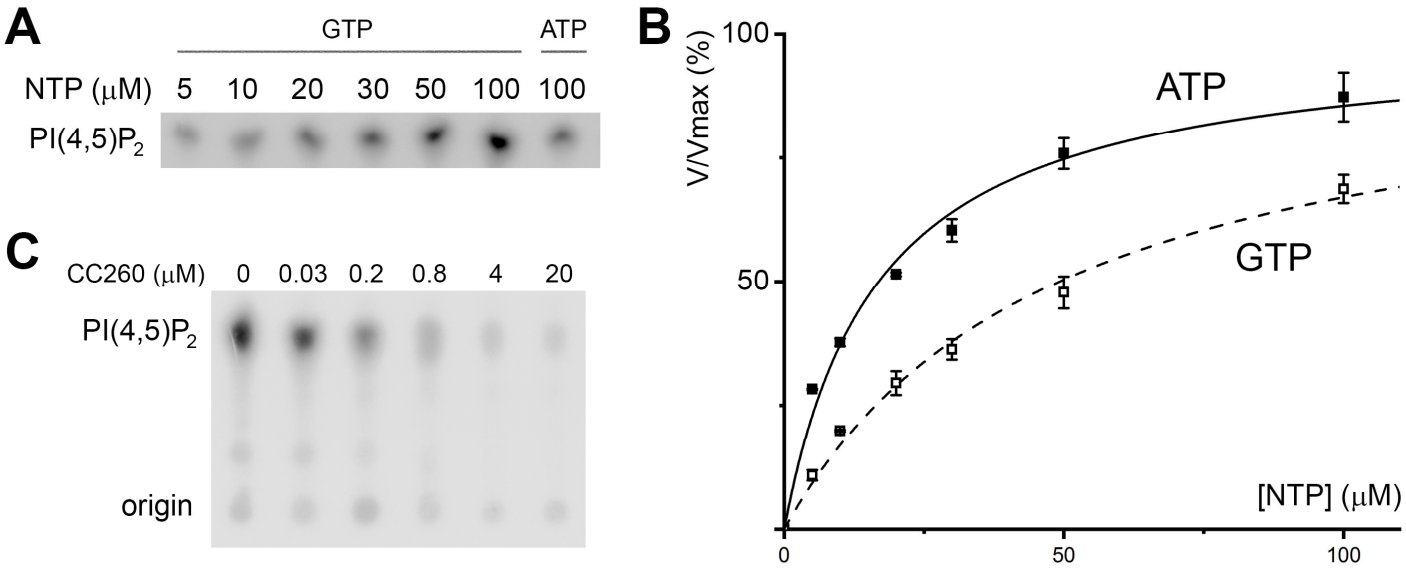
A
GTP
ATP
NTP (μM) 5 10 20 30 50 100 100
PI(4,5)P2
C
CC260 (μM) 0 0.03 0.2 0.8 4 20
PI(4,5)P2
origin
B
V/Vmax (%)
100
50
ATP
GTP
[NTP] (μM)
0
50
100

Figure S11

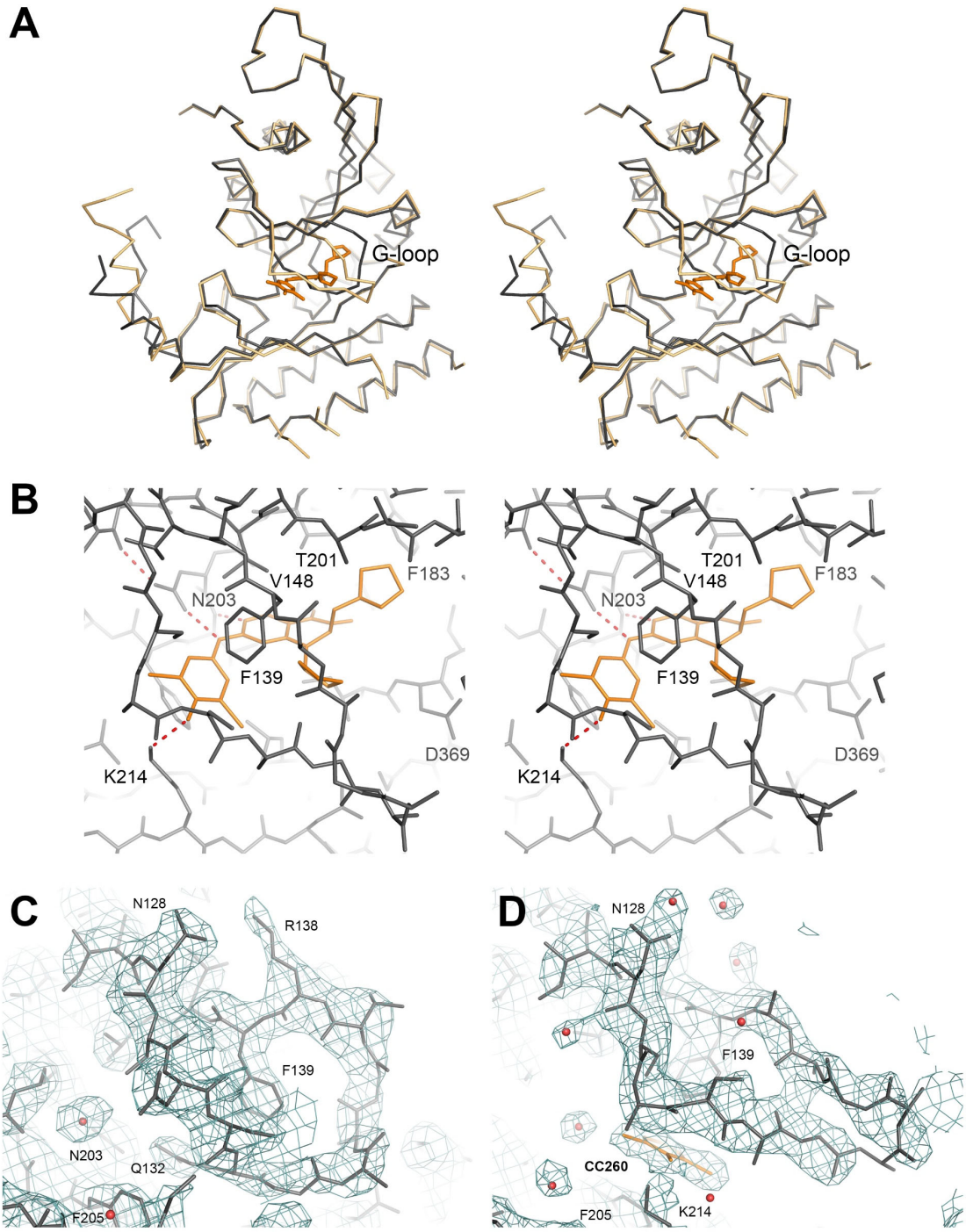
A
G-loop
G-loop
B
T201
V148
F183
N203
F139
D369
K214
T201
V148
F183
N203
F139
D369
K214
C
N128
R138
F139
N203
Q132
F205
D
N128
F139
CC260
F205
K214

Figure S12

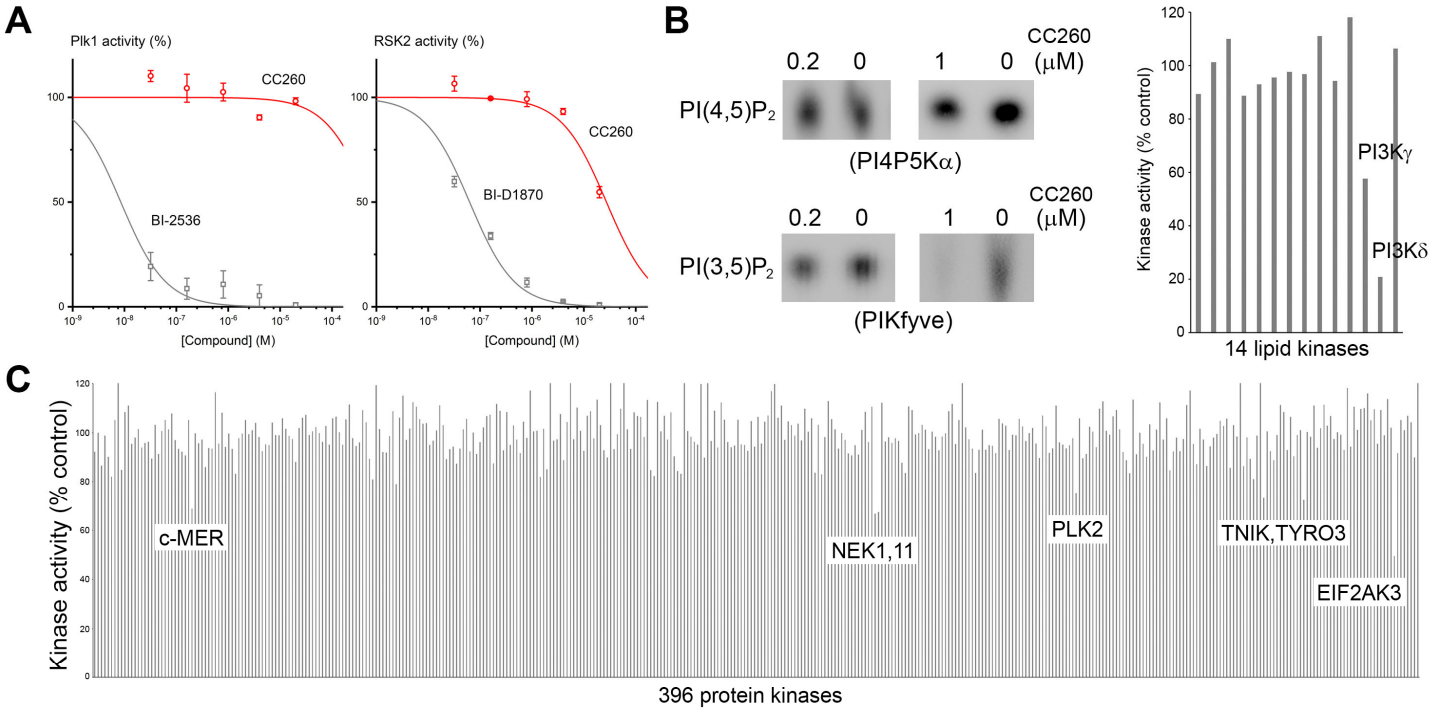

D

	$K_{m,ATP}$ (μM)	$K_{i,CC260}$ (nM)	% inhibition	% inhibition	% inhibition	% inhibition
PI5P4Kα	13	40	39	45	62	76
PI5P4Kβ	17	30	41	58	74	85
PI5P4Kγ	35	600	6	12	22	36
PIKfyve	10	200	6	11	20	33
EIF2AK3	20	230	10	18	30	46
		CC260 (μM)	2.5	5	10	20

Figure S13

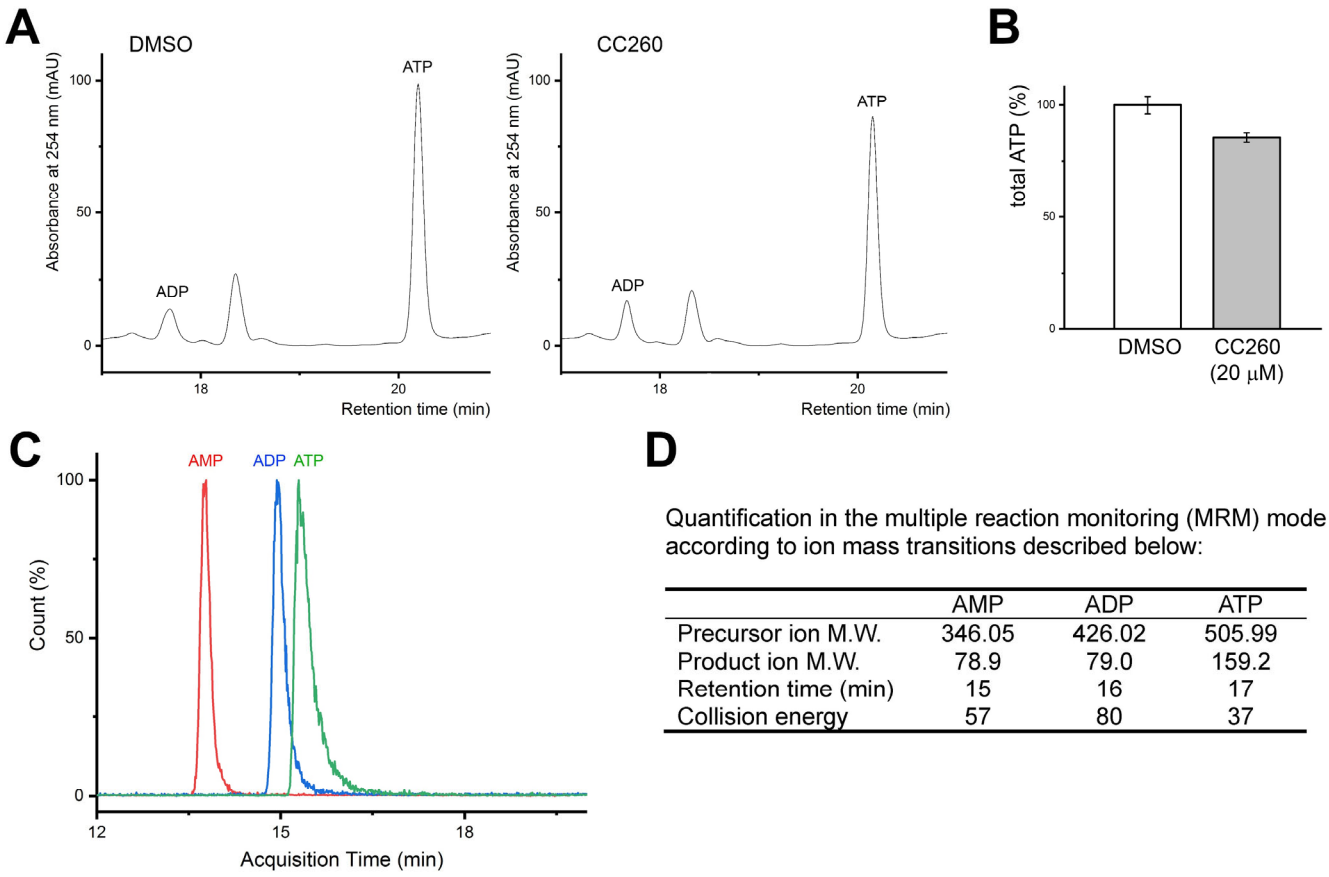

Quantification in the multiple reaction monitoring (MRM) mode according to ion mass transitions described below:

	AMP	ADP	ATP
Precursor ion M.W.	346.05	426.02	505.99
Product ion M.W.	78.9	79.0	159.2
Retention time (min)	15	16	17
Collision energy	57	80	37

Figure S14

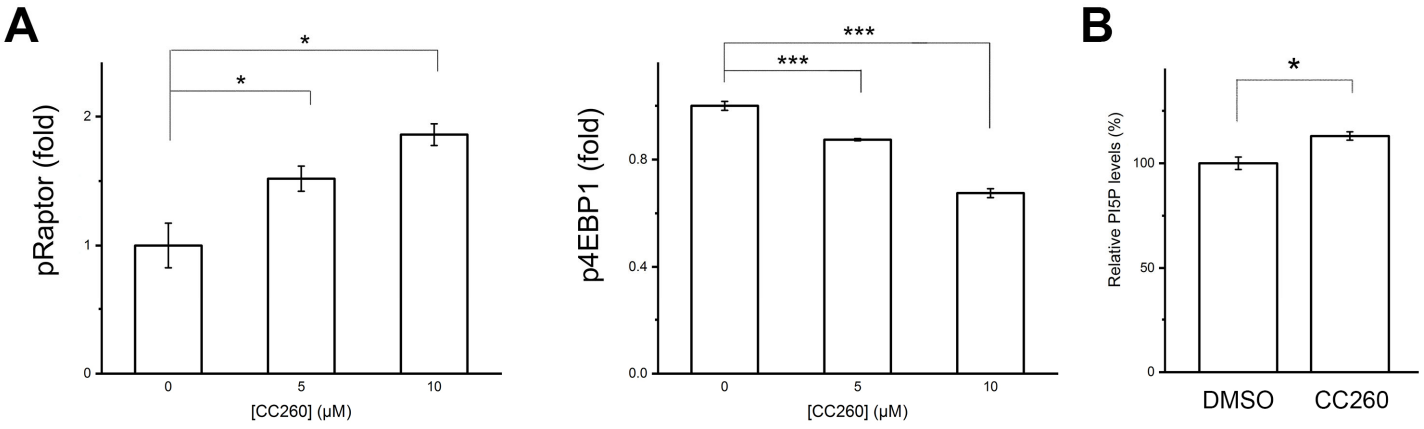
A
pRaptor (fold)
*
*
2
1
0
0
5
10
[CC260] (μM)
p4EBP1 (fold)
***
***
0.8
0.4
0.0
0
5
10
[CC260] (μM)
B
Relative PI5P levels (%)
*
100
50
0
DMSO
CC260

Figure S15

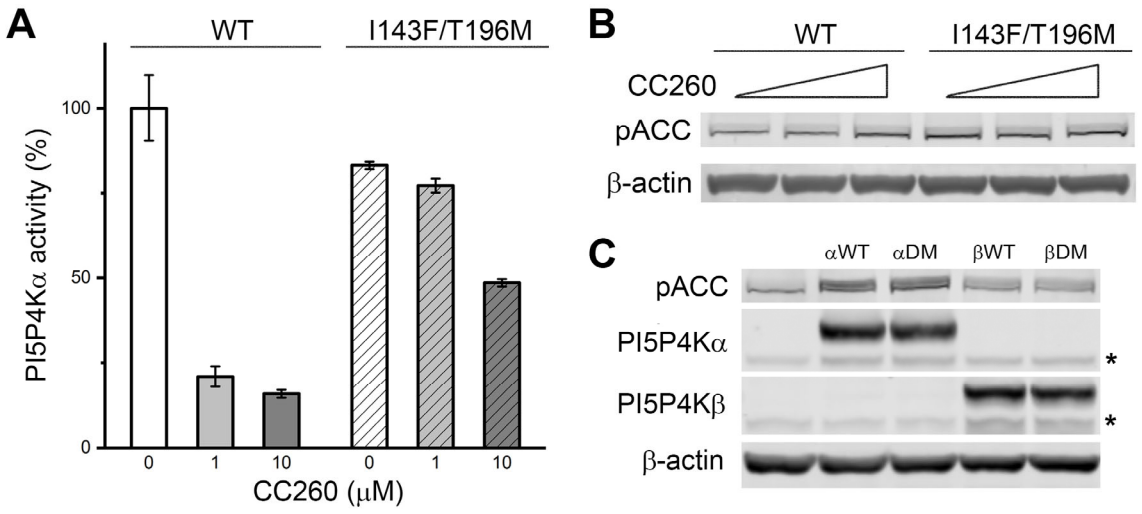
A
WT
I143F/T196M
PI5P4Kα activity (%)
100
50
0
0
1
10
0
1
10
CC260 (μM)
B
WT
I143F/T196M
CC260
pACC
β-actin
C
αWT
αDM
βWT
βDM
pACC
PI5P4Kα
PI5P4Kβ
β-actin
*
*

Figure S16

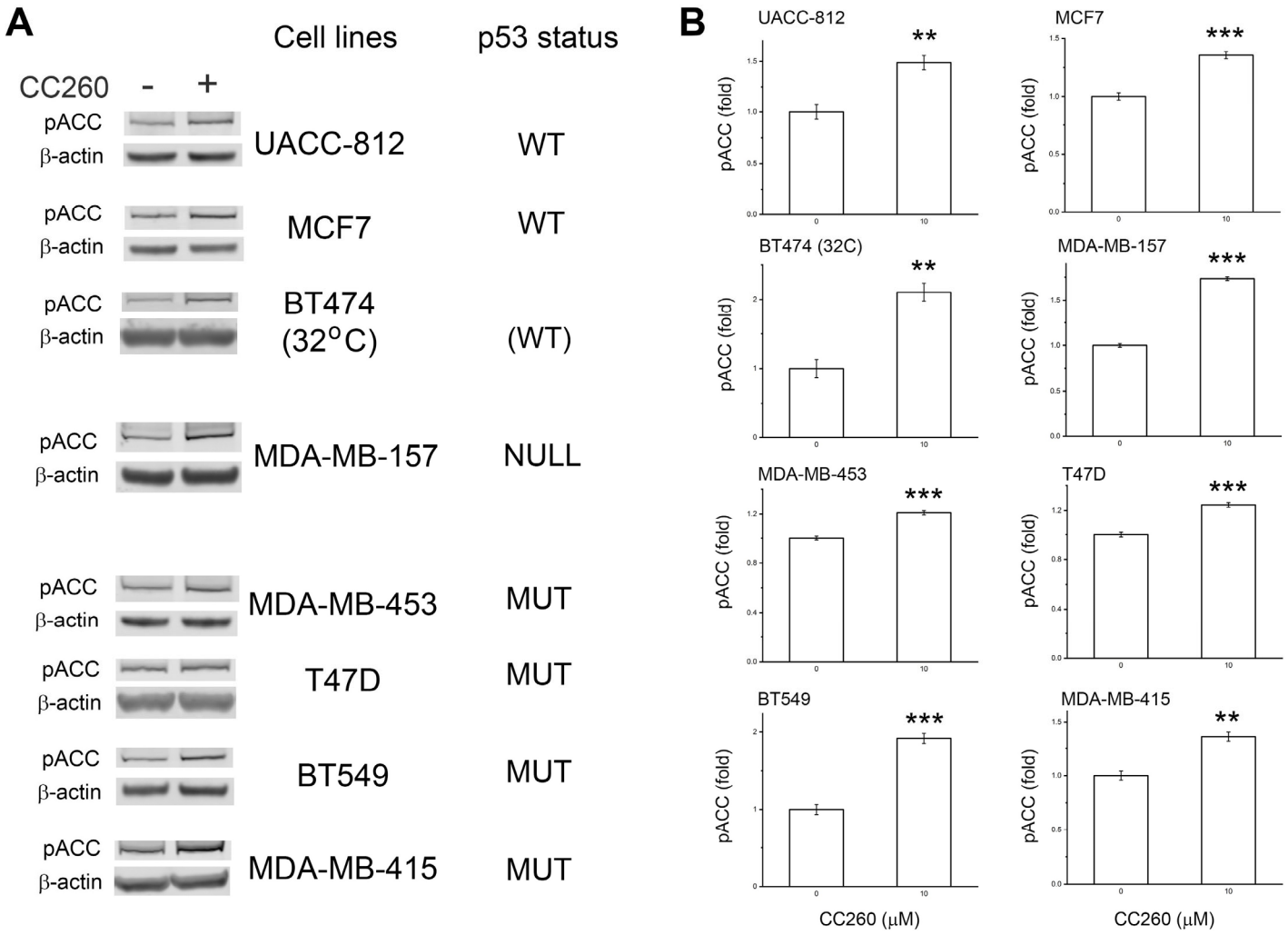
A
Cell lines
p53 status
CC260 - +
pACC
β-actin
UACC-812
WT
MCF7
WT
BT474 (32°C)
(WT)
MDA-MB-157
NULL
MDA-MB-453
MUT
T47D
MUT
BT549
MUT
MDA-MB-415
MUT
B
UACC-812
MCF7
BT474 (32C)
MDA-MB-157
MDA-MB-453
T47D
BT549
MDA-MB-415
pACC (fold)
CC260 (μM)

Figure S17

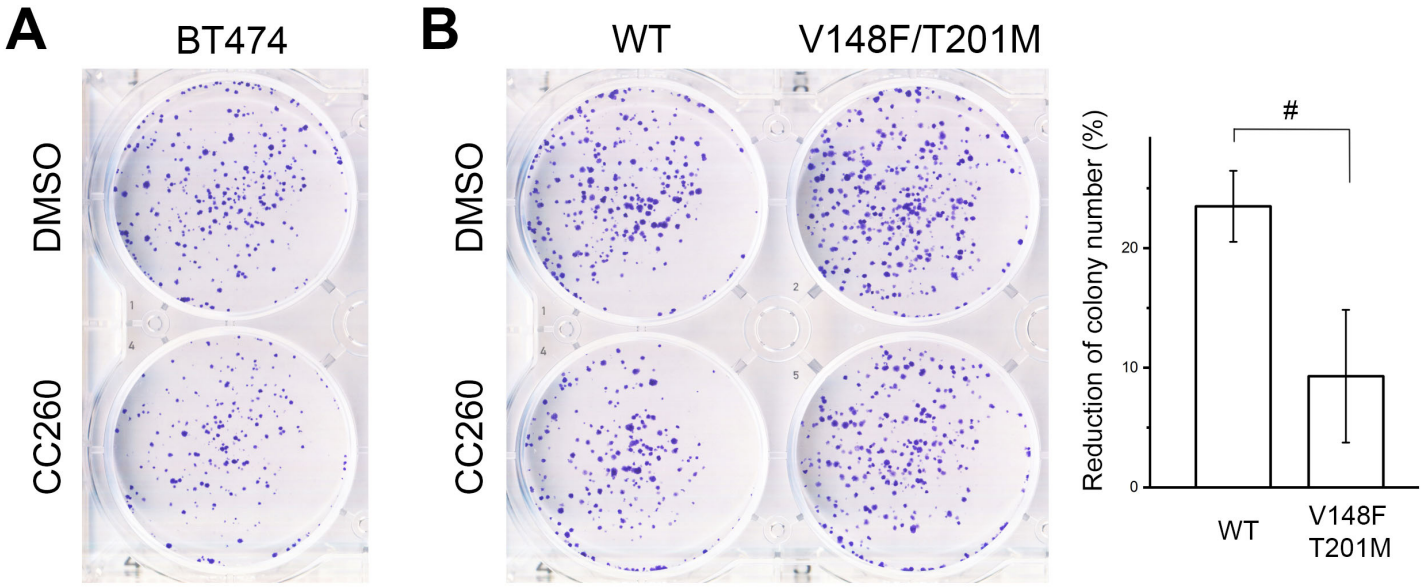
A
BT474
DMSO
CC260
B
WT
V148F/T201M
DMSO
CC260
Reduction of colony number (%)
#
20
10
0
WT
V148F
T201M

Figure S18

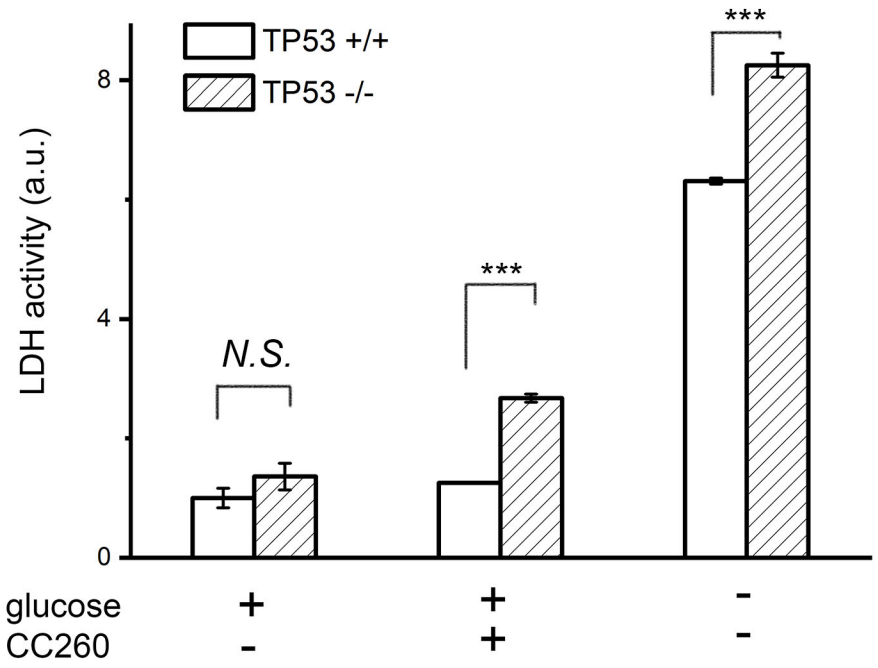

Figure S19

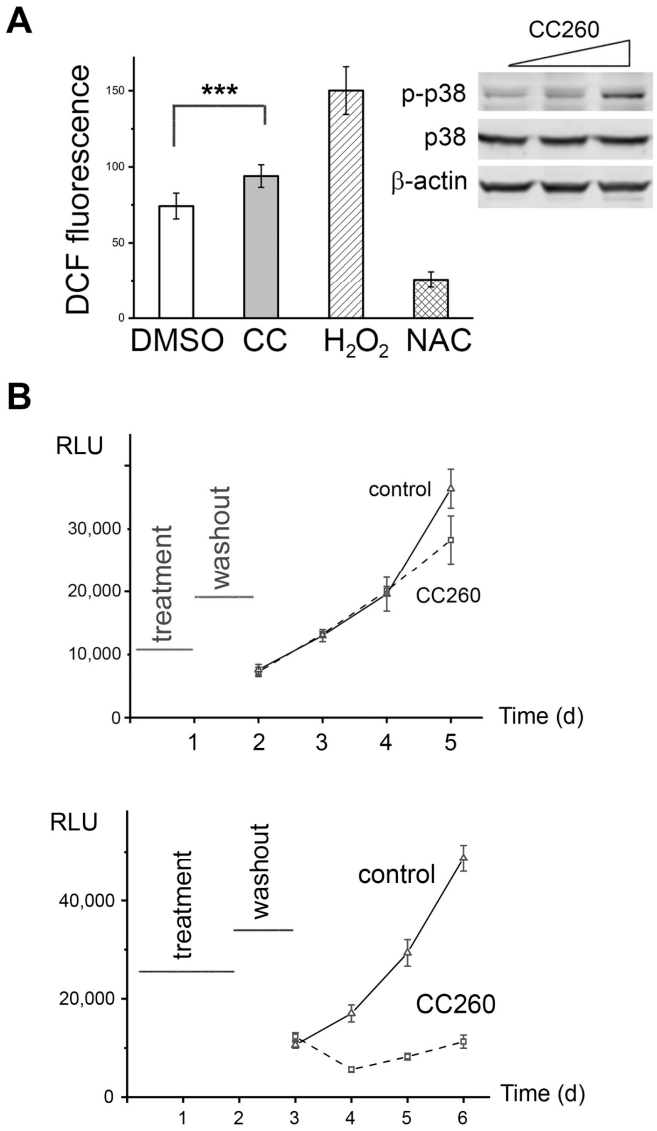
A
CC260
DCF fluorescence
***
p-p38
p38
β-actin
DMSO
CC
H2O2
NAC
B
RLU
treatment
washout
control
CC260
Time (d)
RLU
treatment
washout
control
CC260
Time (d)

Figure S20

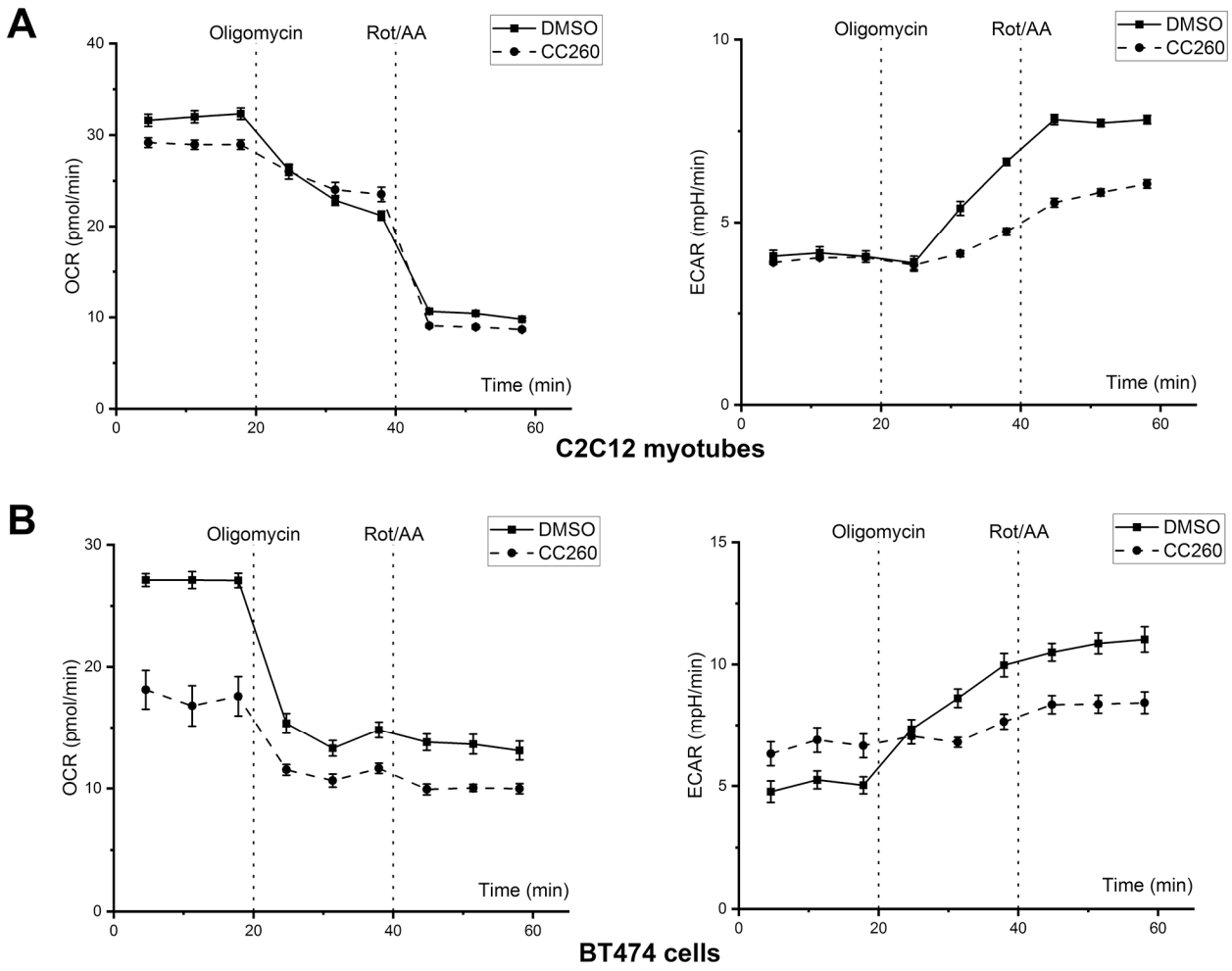
A
Oligomycin
Rot/AA
DMSO
CC260
OCR (pmol/min)
Time (min)
ECAR (mpH/min)
C2C12 myotubes
B
BT474 cells

Figure S21